[Imaging]

The Primer for Sports Medicine Professionals on Imaging: The Shoulder

Nadja A. Farshad-Amacker, MD,*† Sapna Jain Palrecha, MD,† and Mazda Farshad, MD, MPH†

Because of its inherent superior soft tissue contrast and lack of ionizing radiation, magnetic resonance imaging (MRI) is highly suited to study the complex anatomy of the shoulder joint, particularly when assessing the relatively high incidence of shoulder injuries in young, athletic patients. This review aims to serve as a primer for understanding shoulder MRI in an algorithmical approach, including MRI protocol and technique, normal anatomy and anatomical variations of the shoulder, pathologic conditions of the rotator cuff tendons and muscles, the long head of the biceps tendon, shoulder impingement, labral and glenohumeral ligament pathology, MR findings in shoulder instability, adhesive capsulitis, and osteoarthritis.

Keywords: shoulder; MRI; imaging; shoulder anatomy; shoulder pathologies

Magnetic resonance imaging (MRI) is becoming progressively important in daily clinical use because of its ability to visualize soft tissue structures while avoiding harmful radiation exposure. Because of the complex anatomy of the shoulder joint and a high incidence of shoulder structure injuries in young, athletic patients, MRI has become the most important imaging modality.

SHOULDER IMAGING PROTOCOL

Shoulder imaging is implemented with the patient in supine position with their arm in neutral position. Internal rotation of the shoulder should be avoided because of resultant structure overlapping.[8]

The shoulder joint should be imaged in 3 planes: axial, oblique coronal, and oblique sagittal.

Axial images can assess the subscapularis (SSC) tendon; the extra-articular portion of the long head of the biceps tendon (LHBT) with its course along the bicipital groove; the articular cartilage; the labrum (particularly the anterior and posterior labrum); the joint capsule with the superior (SGHL), middle (MGHL), and inferior glenohumeral ligaments (IGHL); the acromioclavicular (AC) joint; and all osseous structures, particularly the humeral head.

Oblique coronal images are obtained parallel to the supraspinatus (SSP) tendon and can assess the SSP and infraspinatus (ISP) tendons, the biceps tendon anchor, the superior and inferior labrum, the articular cartilage, the IGHL with the axillary recess, the AC joint, the osseous structures, and the deltoid muscle.

Oblique sagittal images are obtained parallel to the glenoid surface and provide a survey view of regional muscle differentiations isolated denervation effects as opposed to global disuse atrophy. The oblique sagittal images also disclose the rotator cuff interval with the coracohumeral ligament and the joint capsule, the intra-articular course of the LHBT, glenoid morphology, AC joint, and the morphology of the acromion.

A commonly used shoulder protocol is shown in Table 1.

Proton density-weighted fast spin echo (PDw FSE) sequences primarily evaluate tendons, cartilage, labrum, and ligaments. These sequences provide an advantage over T1-weighted sequences because they are cartilage and fluid sensitive. A magic angle effect is a phenomenon of short time of echo (TE) sequences (like T1w and PDw) and is observed in highly ordered tendons and fibrocartilaginous tissues such as the labrum, that lie in a 55° angle relative to the main magnetic field. This effect produces an increased signal within structures, for instance the SSP tendon approximately 1 cm above the footprint, and thus may be misinterpreted for tendinopathy. As this effect will diminish in TE > 37 ms, it should always be compared with the T2-weighted (T2w) images and note made that magic angle does not have an effect on morphology; thus, the presence of fraying or tear reflect true pathology in the structure of concern.[13,31]

From †Hospital for Special Surgery, New York, New York

*Address correspondence to Nadja A. Farshad-Amacker, MD, MRI Department, Hospital for Special Surgery, 535 East 70th Street, New York, NY 10021 (e-mail: amackern@hss.edu).

The authors report no potential conflicts of interest in the development and publication of this manuscript.

DOI: 10.1177/1941738112468265

Table 1. Shoulder MRI protocol.

Parameters	Oblique Coronal T2w FS FSE	Oblique Coronal PDw FSE	Oblique Sagittal PDw FSE	Axial PDw FSE
TR, ms	4000	4000	4000	4000
TE, ms	60	34	34	34
ETL	13	10	10	10
RBW, kHz	20.83	31.25	31.25	31.25
Field of view	16	16	16	15
Matrix	256 × 224	512 × 384	512 × 224	512 × 384
Slice thickness, mm	3	3	4	3.5
Interslice gap, mm	0	0	0	0
NEX	2	2	2	2

TR, time of repetition; TE, time of echo; ETL, echo trail length; RBW, receiver bandwidth; NEX, number of excitations; PDw FSE, proton density–weighted fast spin echo; T2w FS FSE, T2-weighted fat suppressed fast spin echo.

T2-weighted fat-suppressed fast spin echo (T2w FS FSE) sequences are sensitive for fluid/edema and therefore helpful in detection of edema in the bone marrow or tissue. In the setting of acute trauma, the fat-suppressed images may disclose radiographically occult fractures or extracapsular soft tissue edema in the presence of glenohumeral translation.

In case of MR arthrography, the PDw FSE images are replaced by T1-weighted (T1w) fat-saturated FSE images.[43,53] The application of intra-articular contrast medium showed a relevant increase in sensitivity and specifity for the detection of small SSP tears.[9]

The so-called ABER view (abduction and external rotation arm position) in conventional MRI or MR arthrography has been introduced to increase the sensitivity for detection of articular-sided and horizontal component partial SSP and ISP tears[29,56]; however, its superiority to the standard MR arthrography is not yet defined.[24,49,67]

IMAGING PROTOCOL: PEARLS AND PITFALLS

- Place patient supine, with arm in neutral position
- Images in 3 planes: oblique coronal, oblique sagittal, and axial
- Two sequences used: T2w FS FSE and PDw FSE or MR arthrography with T1w FS FSE instead of PDw FSE
- Magic angle effect may mimic SSP tendinopathy on oblique coronal PDw sequences, comparison with the T2w sequence is necessary

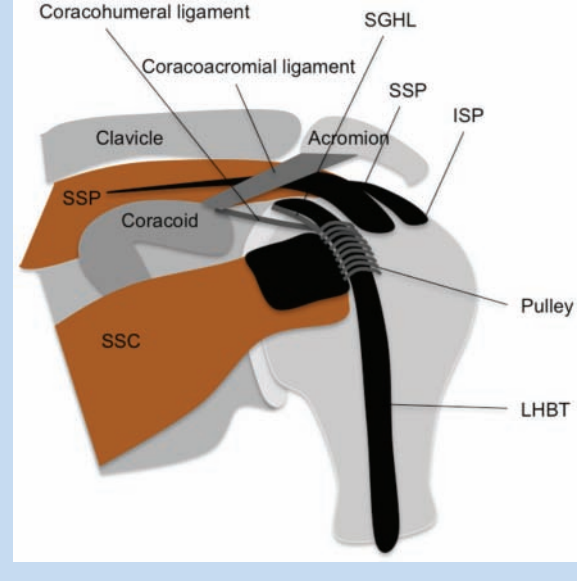

Figure 1. Schematic illustration of the anterolateral shoulder anatomy.

ALGORITHMIC APPROACH TO THE SHOULDER

Tendons and Muscles

Rotator Cuff

Anatomy and normal MR appearance. The subscapularis (SSC), as an internal rotator of the shoulder, originates from the

subscapular fossa and attaches at the lesser tuberosity of the humeral head. At the inferior aspect of the SSC attachment, the tendon becomes very short and the muscle almost directly attaches to the lesser tubercle.[35] Evaluation of the SSC tendon is best performed using the axial and oblique sagittal planes (Figures 1 and 2).

The supraspinatus (SSP) originates from the superior scapular fossa and inserts at the greater tuberosity of the humeral head. It serves as an abductor and suppressor of the humeral head. The SSP tendon is best evaluated in the oblique coronal and oblique sagittal planes. The tendon courses with a 55° angle to the magnetic field and may show hyperintense signal alteration approximately 1 cm above the footprint in the PDw FSE sequence because of the magic angle effect. This effect will diminish in echo times > 37 ms and therefore, if observed, should always be compared with the T2-weighted image (Figures 1 and 3).

The infraspinatus (ISP) as the primary external rotator of the shoulder originates from the inferior scapular fossa and attaches at the greater tuberosity of the humeral head, immediately posterior to the SSP tendon insertion, with the anterior border of the ISP tendon slightly overlapping the posterior border of the SSP tendon.[7] The ISP tendon is best evaluated in the oblique coronal and oblique sagittal planes (Figure 3).

The Teres minor muscle (TM) parallels the ISP as an additional external rotator, has its origin at the posterolateral border of the scapula, and attaches at the greater tuberosity of the humeral head inferior to the ISP tendon. The TM is best evaluated in the axial and oblique sagittal planes. The TM superiorly forms a border of the quadrilateral space, together with the teres major inferiorly, the long head of triceps medially, and the humerus laterally, through which courses the axillary nerve and posterior humeral circumflex vessels[57] (Figures 2 and 3).

The rotator cuff interval is the triangle between the coracoid process, SSC, and the SSP tendon visualized in the oblique sagittal plane (Figure 2b). The coracohumeral ligament (CHL) and the superior glenohumeral ligament (SGHL) are key structures to evaluate within the rotator cuff interval. The CHL originates at the lateral base of the coracoid and extends superior to the biceps tendon and forms the pulley sling together with the SGHL and SSC fibers (Figures 1 and 2).

On MR, a normal, healthy tendon should appear with low signal intensity on all sequences (Figures 2 and 3).

The rotator cuff muscles are best evaluated in the oblique sagittal plane (Figure 4). A normal healthy muscle should have homogenous intermediate signal intensity on MRI.

Pathologies of the rotator cuff. Tendinopathy/tendinosis histopathologically refers to tendon degeneration with collagen alterations including fiber disorientation, increased intrasubstance deposition of mucoid, and absence of inflammatory cells (thus the term *tendinitis* is inappropriate).[27]

Criteria for tendinopathy in MR are a (1) thickened tendon with (2) hyperintense signal alteration predominantly in T1w or PDw FSE and corresponding slightly increased signal intensity in T2w images but not reaching a fluid signal.[25,28,39] Tendons may also form soft tissue ganglion that are of fluid intensity, and these cysts often decompress secondarily into the rotator cuff footprint, forming intraosseous cysts (Figure 5).

Calcific tendinopathy is caused by deposition of calcium hydroxyapatite within the tendon. It is present in up to 20% of adults but only one third of those are symptomatic.[54] It most commonly occurs in the SSP tendon followed by the ISP and SSC tendons. Calcium deposits are best evaluated on plain radiographs. On MRI, identification of the calcium deposits with low signal intensity within the hypointense tendon is very challenging and may lead to either false positive or false negative readings.[68] Tendon irritation can accompany calcium deposits within the tendon, and as such, might be detected as perifocal edema in T2w sequences[23] (Figure 6).

Rotator cuff tears. In general, tendon tears are classified into complete or partial tears. This general classification differs for the rotator cuff tendons, particularly for the ISP and SSP tendon tears, as these are more precisely classified into full-thickness versus various partial-thickness tears (articular, intratendinous, and bursal-sided). The width of the tear can be further described as percentage to the tendon.

SSP tendon tears. A full-thickness SSP tear allows communication between the articular and the bursal compartment. Although rare, a full-width, full-thickness SSP tear with disruption of all tendon fibers is expected to result in retraction of the musculotendinous unit (Figure 7); a small full-thickness tear may not result in tendon retraction (Figure 8a).

Partial-thickness SSP tears are divided based on their location: articular-sided (Figure 8b), intrasubstance, or bursal-sided tears (Figure 8c). The extent of the partial tear can further be declared according to the depth; a commonly used grading system is: Grade I for tears < 3 mm, Grade II for extension > 3 mm but < 50% of the tendon thickness, and Grade III if > 50% of tendon thickness is involved.[12] Tears of the SSP tendon most commonly arise at the ventral aspect of the tendon immediately to its attachment and can expand dorsally into the ISP tendon or ventrocaudally into the SCC tendon.[3,43]

The partial articular-sided SSP tendon avulsion (PASTA) lesion is located immediately at the footprint (Figure 8b) and is often seen in young athletes with repetitive overhead activities.[48] The reverse PASTA, in contrast, corresponds to a bursal-sided partial tear at the SSP footprint.[48]

ISP tendon tears are often associated with SSP tears and may be observed in younger athletes with overhead activities and posterosuperior impingement, in which there is often an articular side delamination of the cuff (Figures 9 and 16).

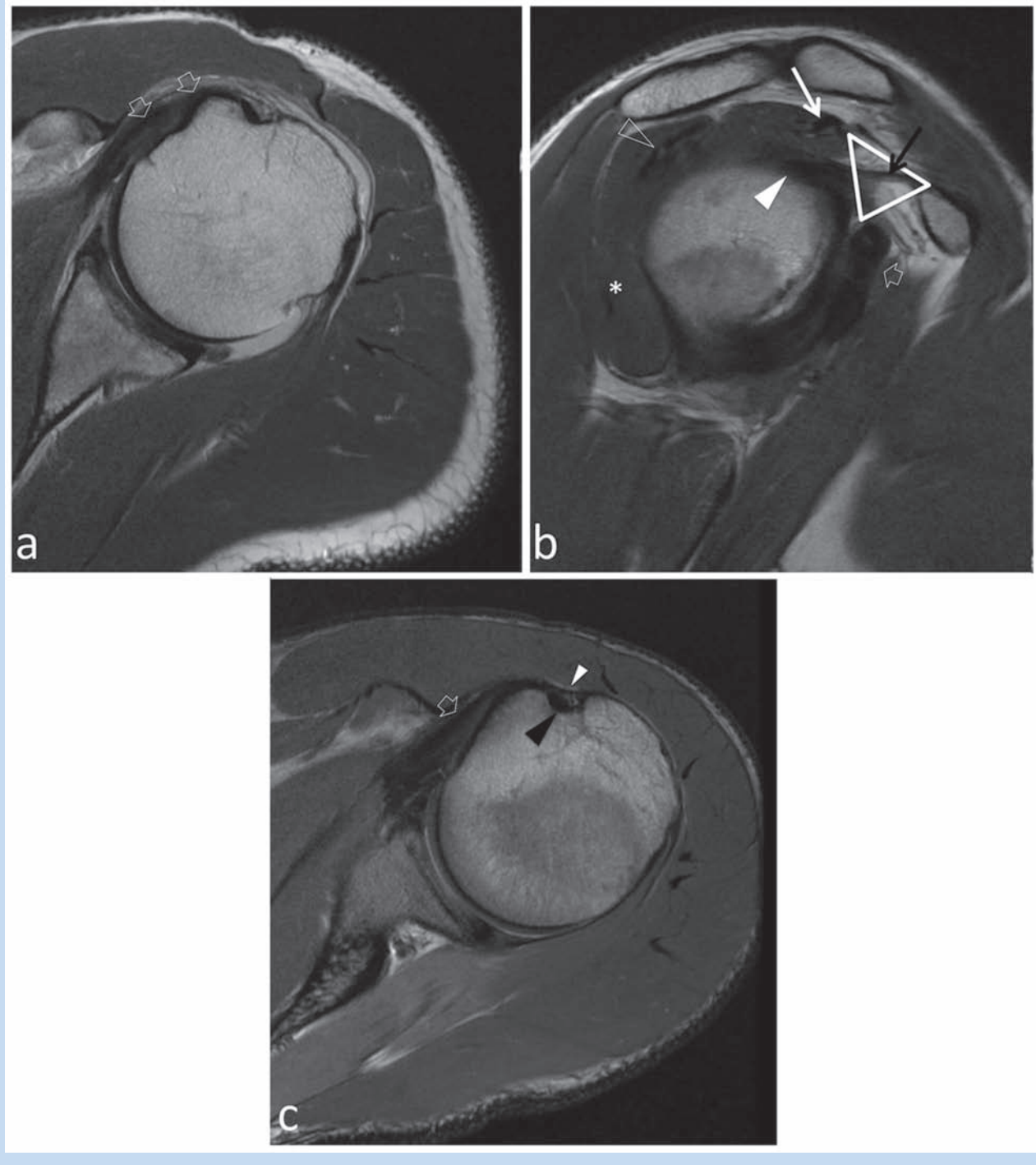

Figure 2. Normal anatomy of the SSC tendon and LHBT. (a) Axial PDw FSE shows the insertion of the SSC tendon (open arrows). (b) Oblique sagittal PDw FSE image shows all the rotator cuff muscles with their tendons; the SSC tendon (open arrow), the SSP tendon (white arrow), the ISP (open arrowhead), and the TM tendon (*), the intra-articular LHBT with the biceps anchor (arrowhead), and the rotator cuff interval (triangle) with the CHL (black arrow). (c) The axial PDw FSE image shows the LHBT at its entrance in the bicipital groove (black arrowhead) held by the pulley (white arrowhead), formed by the CHL, the SGHL, and the SSC tendon (open arrow). SSC, subscapularis; LHBT, long head of biceps tendon; PDw FSE, proton density–weighted fast spin echo; SSP, supraspinatus; ISP, infraspinatus; TM, teres minor muscle; CHL, coracohumeral ligament; SGHL, superior glenohumeral ligament.

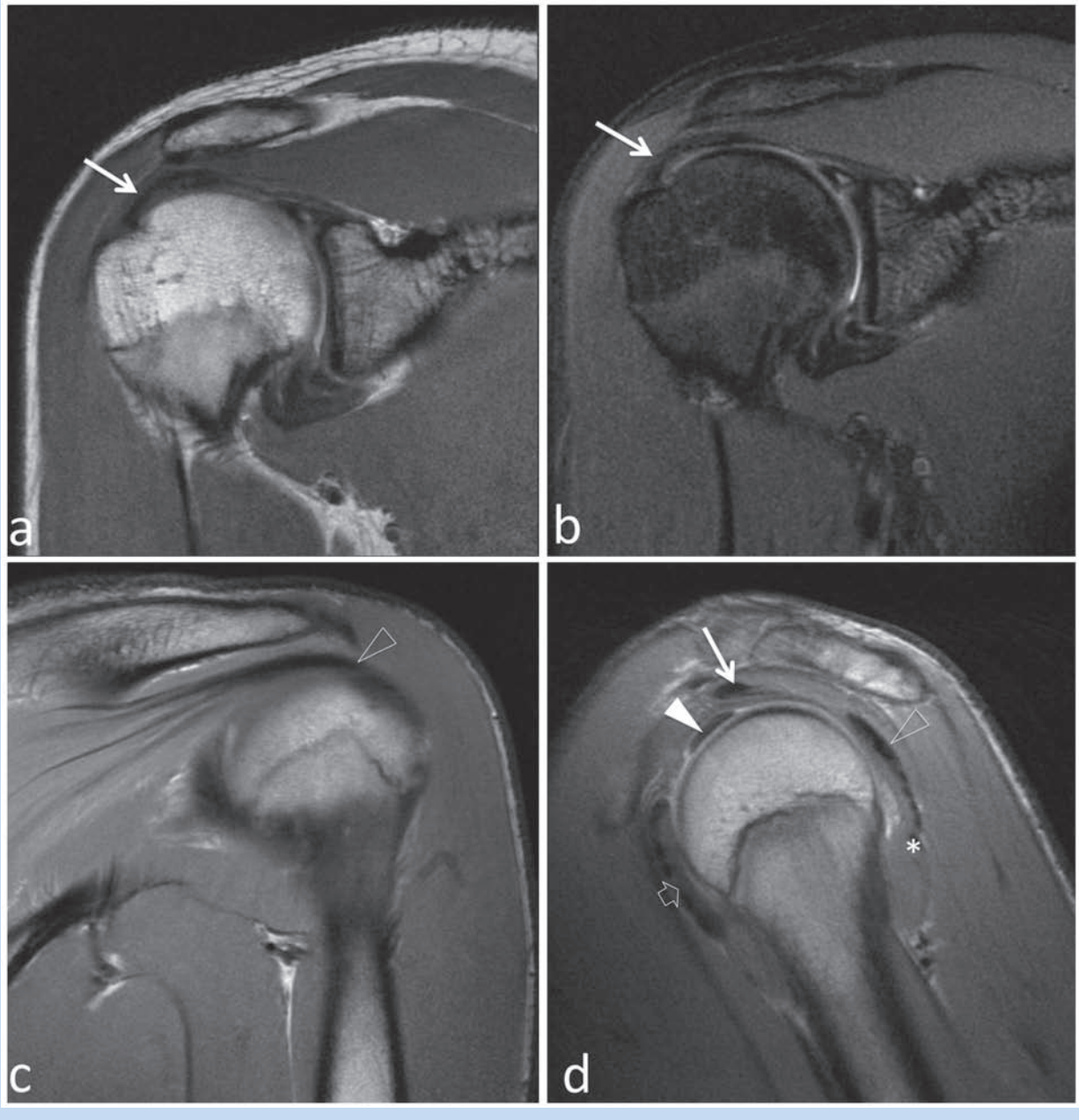

Figure 3. Normal anatomy of the rotator cuff tendons, with focus on the SSP and ISP. Oblique coronal (a) PDw FSE and (b) T2w FS FSE images show a normal appearance of the SSP tendon (arrow). (c) Oblique coronal PDw FSE image shows normal appearance of the ISP tendon (open arrowhead). (d) Oblique sagittal PDw FSE image shows all the rotator cuff muscles with their tendons and the intra-articular LHBT (arrowhead); the SSC tendon (open arrow), the SSP tendon (arrow), the ISP (open arrowhead), and the TM tendon (*). SSP, supraspinatus; ISP, infraspinatus; PDw FSE, proton density–weighted fast spin echo; T2w FS FSE, T2-weighted fat-suppressed fast spin echo; LHBT, long head of biceps tendon; SSC, subscapularis; TM, teres minor muscle.

TM tendon tears are rare and present most commonly as partial tears accompanied by ISP tears.

SSC tendon tears can be isolated or accompanied by other rotator cuff tendon tears, such as the SSP tendon.[17] The highest sensitivity and specificity for the evaluation of SCC tendon tears has been achieved by combined assessment of the axial and oblique sagittal planes.[42] Tears of the SSC are often associated with LHBT subluxation or dislocation of the bicipital groove (Figure 10).

Subluxation of the LHBT, particularly if located within or posterior to the SSC tendon, is a very specific but insensitive sign for SSC tears.[39,42,61]

Figure 4. (a) Oblique sagittal PDw FSE image shows normal anatomy and signal intensity of all the rotator cuff muscles with their tendons in a 17-year-old patient; SSC (open arrows), SSP (arrow), ISP (arrowhead), and TM (*). The tangent sign[66] is considered negative (line). (b) Oblique sagittal PDw FSE image shows an atrophied SSP muscle with a corresponding positive tangent sign (line) and fatty degeneration (Goutallier Stage II[20]) in a 29-year-old patient. PDw FSE, proton density–weighted fast spin echo; SSC, subscapularis; SSP, supraspinatus; ISP, infraspinatus; TM, teres minor muscle.

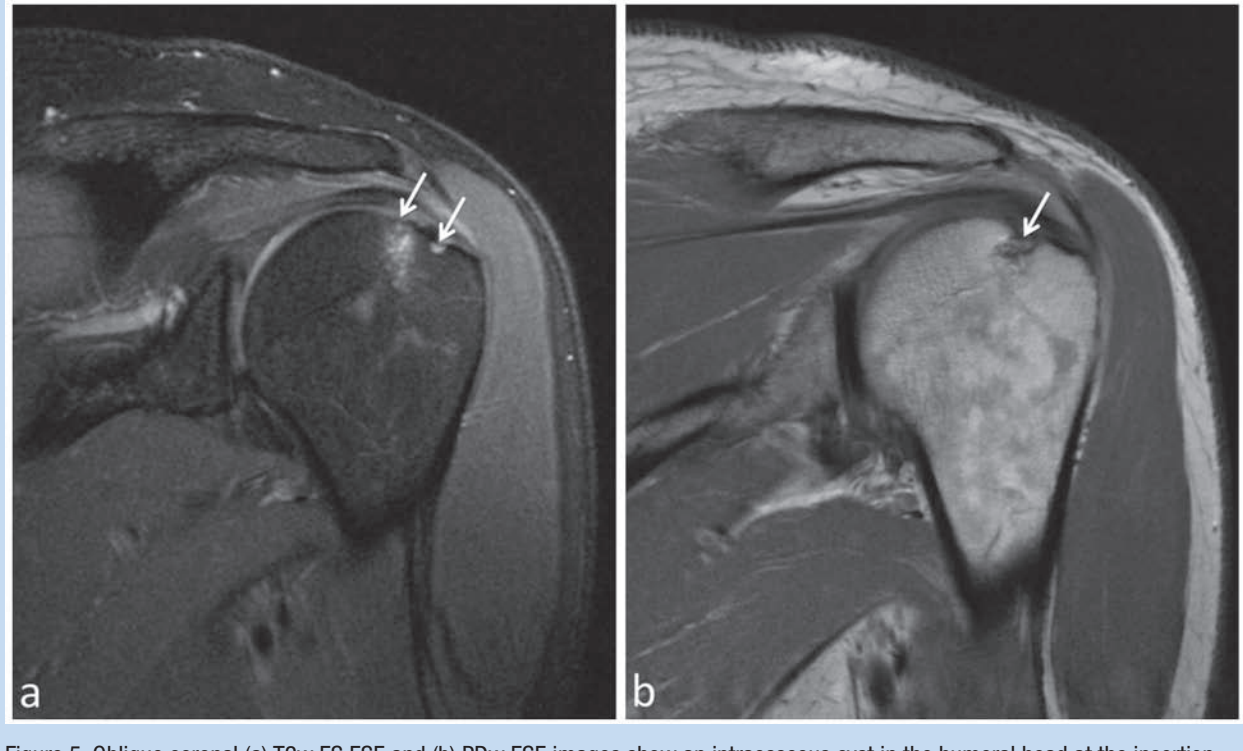

Figure 5. Oblique coronal (a) T2w FS FSE and (b) PDw FSE images show an intraosseous cyst in the humeral head at the insertion of the anterior fibers of the ISP tendon in a 47-year-old patient. T2w FS FSE, T2-weighted fat-suppressed fast spin echo; PDw FSE, proton density–weighted fast spin echo; ISP, infraspinatus.

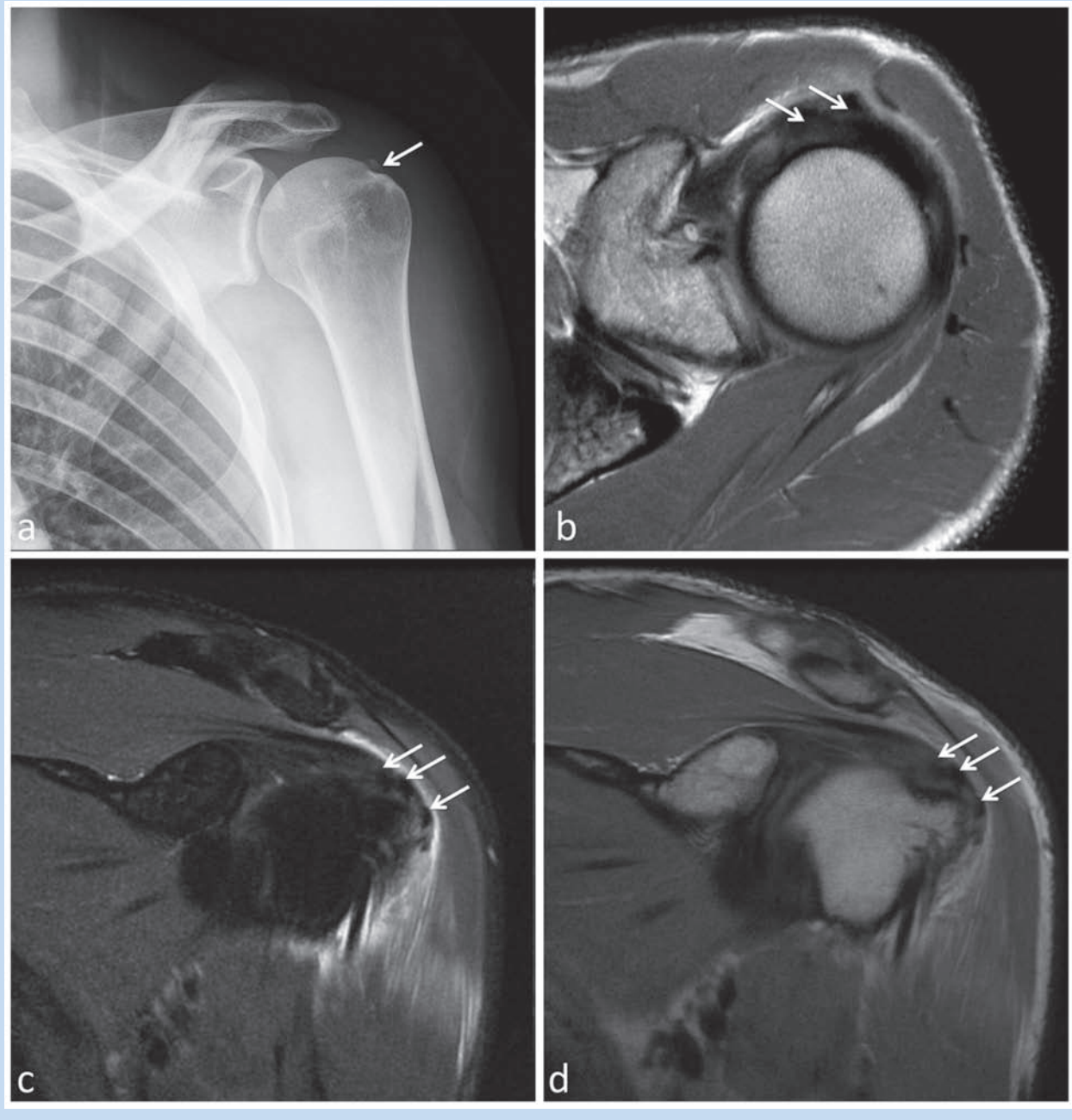

Figure 6. Calcific tendinopathy of the SSP tendon in a 43-year-old patient. (a) Radiograph in external rotation shows calcium hydroxyapatite deposits in projection to the SSP tendon (arrow). On MR, (b) axial PDw FSE sequence, oblique coronal, (c) T2w FS FSE, and (d) PDw FSE images were able to detect the calcium deposits within the SSP tendon (arrow). Note the ruptured bursa due to the inflammatory response. SSP, supraspinatus; PDw FSE, proton density–weighted fast spin echo; T2w FS FSE, T2-weighted fat-suppressed fast spin echo.

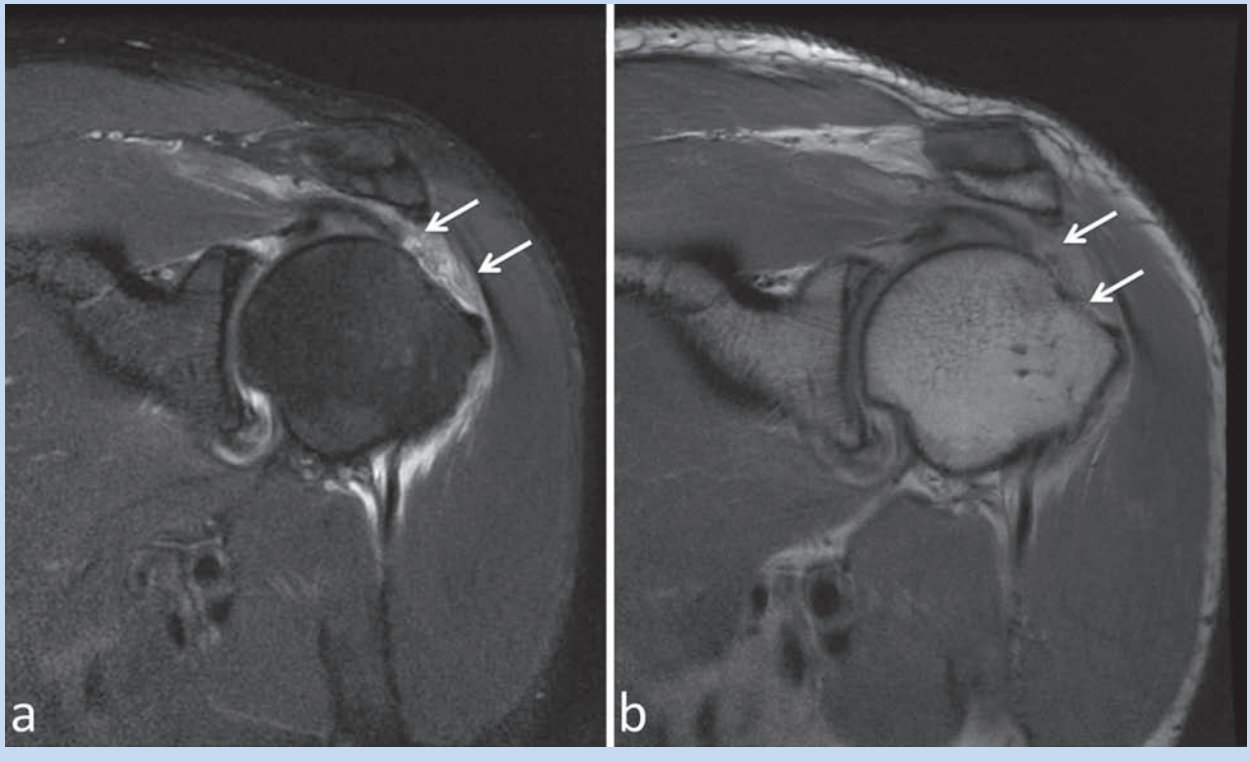

Figure 7. A complete full-thickness SSP tear with tendon retraction (arrows) in a 53-year-old patient is shown on oblique coronal (a) T2w FS FSE and (b) PDw FSE images. SSP, supraspinatus; T2w FS FSE, T2-weighted fat-suppressed fast spin echo; PDw FSE, proton density–weighted fast spin echo.

Secondary signs of rotator cuff tears are tendon retraction, fluid in subdeltoid-subacromial bursa, fatty muscle degeneration or atrophy, and superior humeral migration (Figures 4b, 7, and 10b).

ROTATOR CUFF TEARS: PEARLS AND PITFALLS

- SSP and ISP are best evaluated in oblique coronal and oblique sagittal planes
- Generally, tendon tears are classified as partial or complete tears
- Tear classification for SSP has become more specified into full-thickness and partial-thickness (articular, bursal, and intrasubstance) tears
- Assessment in the axial plane is most sensitive in evaluation of SSC tendon pathology; its specificity is increased with additional oblique sagittal imaging
- Biceps dislocation is specific for SSC tears, particularly if the LHBT is located posterior to the SSC tendon
- Calcific tendinopathy is best visualized on plain radiographs

Rotator cuff muscles evaluation. Muscles should be evaluated for (1) fatty infiltration, (2) atrophy, and (3) edema.

Qualitative assessment of the fatty degeneration of the rotator cuff muscles can be made using the Goutallier classification. The Goutallier classification (Table 2) was initially described for CT[20] and later adapted for MR.[14]

Muscle atrophy of the SSP is detected by drawing a tangent between the coracoid and the scapular spine. If the SSP muscle extends superior to this line, the "tangent sign" is negative; if the SSP muscle extends below that line it is considered positive.[66] In the latter case, the muscle is atrophied (Figure 4b).

Denervated muscles present on MRI as hyperintense signal alteration in fluid-sensitive sequences (eg, the T2w sequence) caused by edema (Figure 11). Muscle denervation ultimately results in fatty atrophy. In case of denervation edema or fatty degeneration of both the SSP and ISP muscles, the suprascapular notch should be evaluated for impingement of the suprascapular nerve. With isolated ISP atrophy, the spinoglenoid notch should be assessed for compressive lesions. Isolated edema/atrophy of the TM muscle may be detected with axillary nerve entrapment in the quadrilateral space. This may be accompanied by edema/atrophy of the deltoid

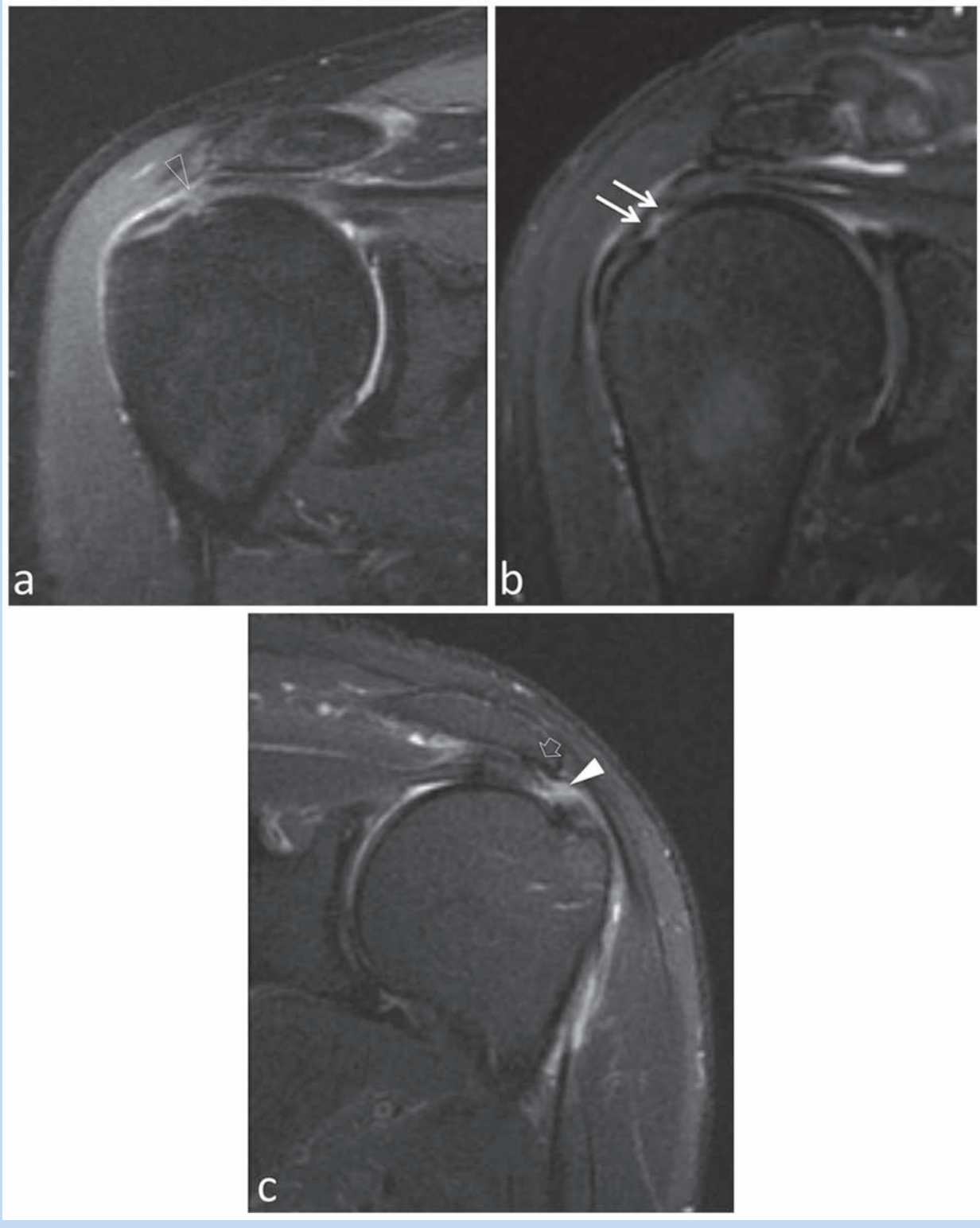

Figure 8. Oblique coronal T2w FS FSE images show (a) a small full-thickness SSP tear (open arrowhead) in a 67-year-old patient, (b) a PASTA lesion (arrows) in 75-year-old patient, and (c) a bursal-sided partial-thickness (> 50% of tendon thickness) SSP tendon tear (arrowhead) in a 56-year-old patient with subacromial impingement by lateral down-sloping of the acromion and a small subacromial spur (open arrow). T2w FS FSE, T2-weighted fat-suppressed fast spin echo; SSP, supraspinatus; PASTA, partial articular-sided SSP tendon avulsion.

Figure 9. Coronal oblique (a) T2w FS FSE and (b) PDw FSE images show an articular-sided partial ISP tear (arrows) in a 53-year-old patient. T2w FS FSE, T2-weighted fat-suppressed fast spin echo; PDw FSE, proton density–weighted fast spin echo; ISP, infraspinatus.

muscle. Isolated denervation of the TM is the most common subselective denervation pattern in the shoulder; it alone does not indicate quadrilateral space syndrome.[53]

ROTATOR CUFF MUSCLES: PEARLS AND PITFALLS

- Best evaluated in oblique sagittal plane
- Goutallier classification for qualitative assessment of fatty infiltration
- Tangent sign (coracoid-scapular spine line) for quantification of SSP muscle atrophy
- Denervation results in muscle edema when acute and atrophy and fatty infiltration when chronic

Long Head of Biceps Tendon and Anchor

Anatomy and normal MR appearance. The LHBT arises at the superior rim of the glenoid (supraglenoid tuberosity) and forms together with the superior labrum and SGHL, the biceps anchor, or biceps-labral complex (Figures 1, 2, and 12a). The tendon initially courses intra-articularly between the SSP and SSC tendon and is best evaluated in the oblique sagittal plane (see Figures 2b and 3d). After entering the bicipital groove, the tendon is considered extra-articular and is best evaluated in the axial plane (see Figure 2c). The tendon is held in the bicipital groove by a fibrous sling surrounding the tendon, namely, the pulley. The pulley is mainly formed by the coracohumeral ligament, the SGHL, and some superior fibers of the SSC tendon[19,63] (see Figures 1 and 2c). The distal biceps attachment at the radial tuberosity is normally not visible on a normal shoulder protocol.

The normal MR signal appearance of the tendon should be low on all pulse sequences.

Pathologies of the LHBT. The MR signal characteristics of the LHBT are similar to that of the rotator cuff tendons.

Tendinopathy/tendinosis is best described as a thickened PDw or T1w hyperintense intratendinous signal without high signal alterations in the T2w images.[67]

A partial tear is defined as T2w hyperintense, T1w iso- to hypointense signal alterations.

A complete tear is defined by tendon retraction to the bicipital groove and absence of the tendon intra-articular on the oblique sagittal plane.[67]

Subluxation or dislocation of the LHBT requires disruption of at least the deep fibers of the "pulley" that are mainly created by the SSC tendon insertion.[19] A dislocation of the LHBT is almost always accompanied with some form of SSC lesion[42,61] (see Figure 10).

LONG HEAD OF BICEPS TENDON: PEARLS AND PITFALLS

- Evaluate the intra-articular part in oblique sagittal plane and the extra-articular part (within the bicipital groove) in the axial plane
- Biceps subluxation/dislocations are associated with pulley lesions and thus almost always accompanied with SSC lesions

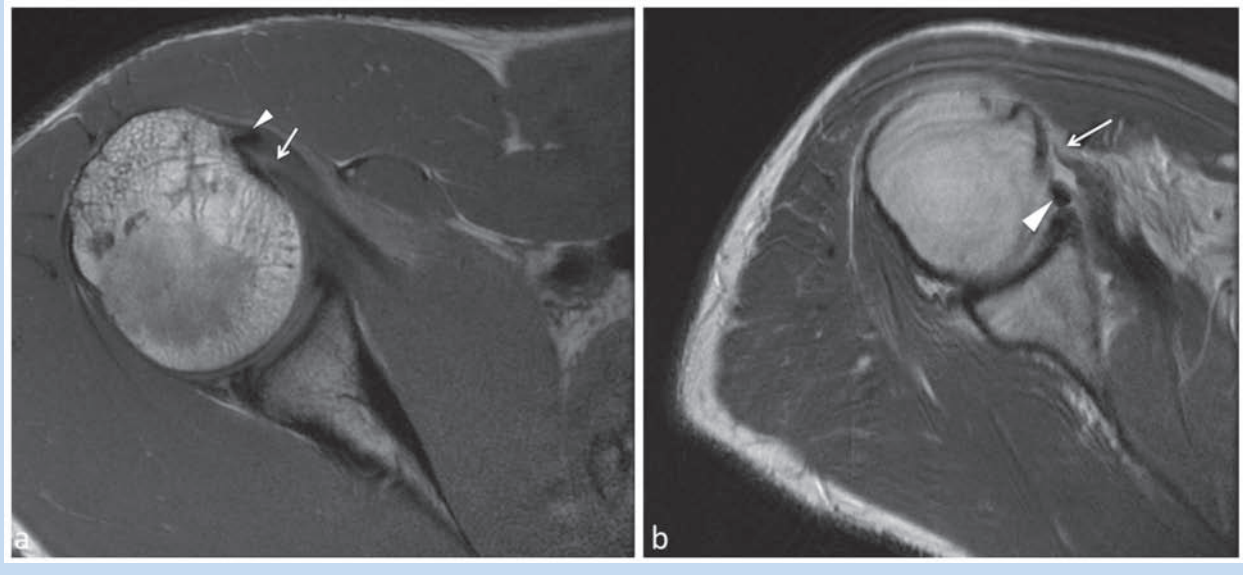

Figure 10. The axial PDw FSE images show pulley lesions (a) with subluxation of the LHBT (arrowhead), delaminating into the SSC tendon (arrow) in a 20-year-old patient and (b) a full-thickness SSC tendon tear (arrow) with dislocation of the LHBT (arrowhead) in a 60-year-old patient. PDw FSE, proton density–weighted fast spin echo; LHBT, long head of biceps tendon; SSC, subscapularis.

Table 2. Goutallier classification.[20]

Goutallier Stage	Findings in Computed Tomography
Stage 0	Normal muscle without fat
Stage I	Few fatty streaks within the muscle
Stage II	Less fat than muscle within the muscle
Stage III	Same amount of fat and muscle within the muscle
Stage IV	More fat than muscle within the muscle

Shoulder Impingement

Impingement syndromes of the shoulder are clinical rather than imaging diagnoses. MRI can disclose anatomical changes that can lead to impingement. Impingement can be divided into external and internal. External impingement is subacromial or subcoracoid. Internal impingement is caused by intra-articular structures.

External impingement. Subacromial impingement is compression of the rotator cuff tendons between the coracoacromial arch (acromion and the coracoacromial ligament) and humeral head. This may be caused by (1) certain acromion shapes, (2) AC joint degenerative changes, (3) a subacromial spur, (4) an os acromiale, or (5) a hypertrophied coracoacromial ligament[25,50,58] (Figures 8c and 13). Subacromial impingement is associated with anterior down-sloping (described by Bigliani, Figure 14) and by lateral down-sloping of the acromion.[4,30]

Subacromial-subdeltoid bursitis is often found in subacromial impingement but can also be associated with rotator cuff pathology or inflammatory disorders.

Subcoracoid impingement is narrowing of the space between the humeral head and the coracoid with consequent compression to the SSC tendon (Figure 15) and less often of the LHBT and CHL. This impingement is caused by (1) a congenitally enlarged or laterally tapered coracoid, (2) a coracoid fracture, or (3) an iatrogenic postsurgical deformity.[15,25] Further compression of the SSC may be seen in the presence of proliferative bone formation at the lesser tuberosity.

Internal impingement. The posterosuperior impingement is defined as compression of the posterior fibers of the SSP tendon and/or as anterior fibers of the ISP tendon between the humeral head and the posterior glenoid.[18] This is seen in young throwing athletes with repetitive overhead motion.[3,60] MR findings include:

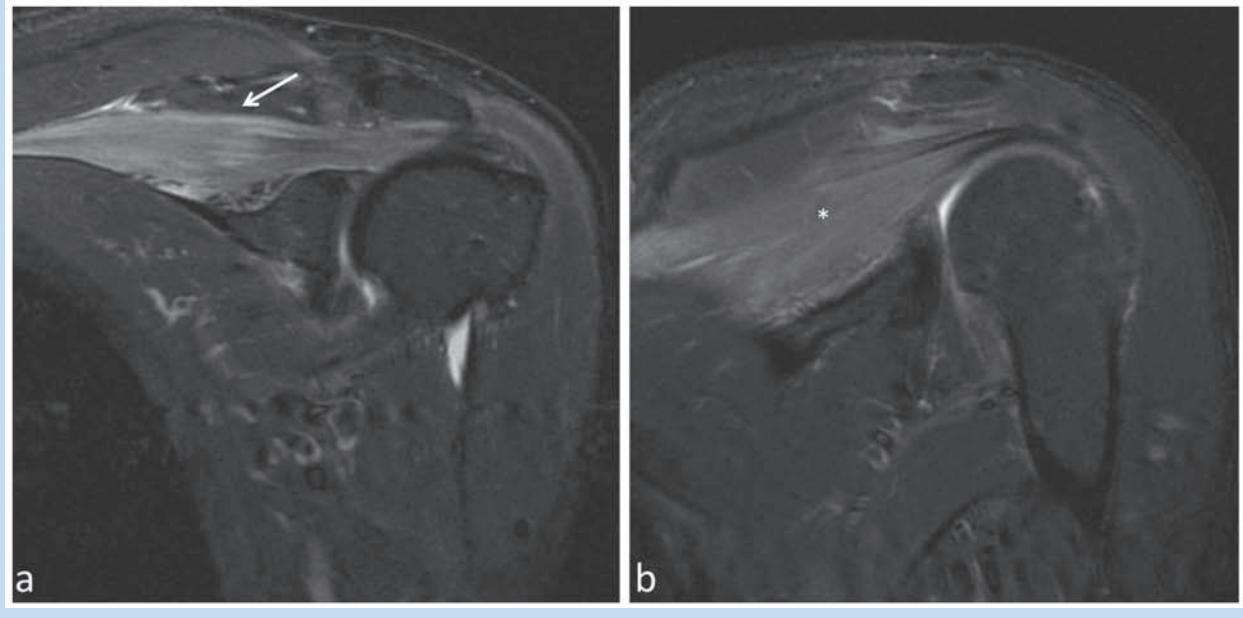

Figure 11. Coronal T2w FS FSE images show denervation edema in the (a) SSP and (b) ISP muscle. T2w FS FSE, T2-weighted fat-suppressed fast spin echo; SSP, supraspinatus; ISP, infraspinatus.

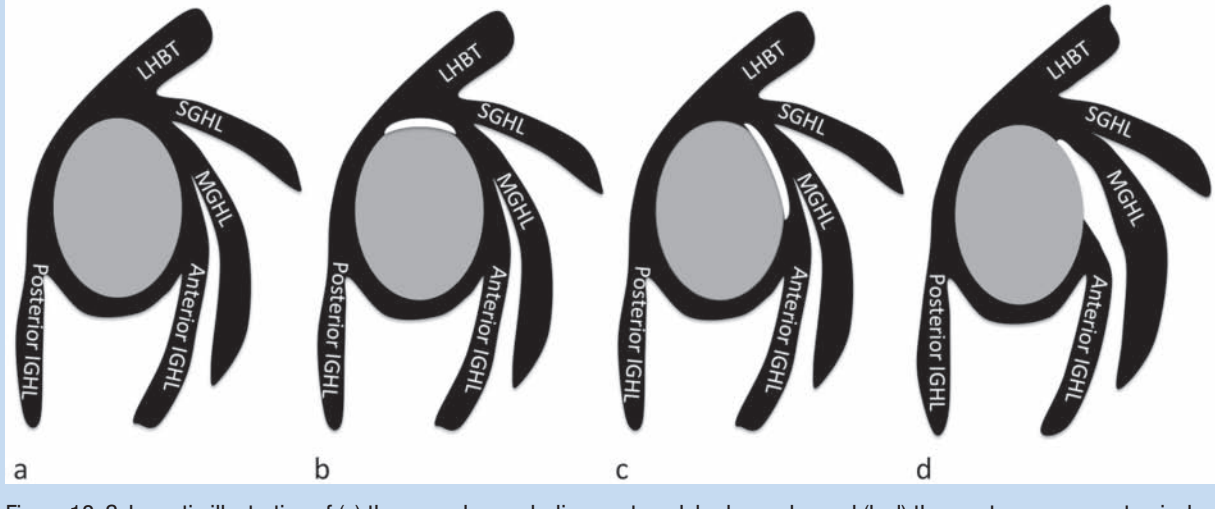

Figure 12. Schematic illustration of (a) the normal capsulo-ligamentous-labral complex and (b-d) the most common anatomical variations. (b) Superior labral recess, (c) sublabral foramen, and (d) the Buford complex.

(1) posterosuperior labrum tear, (2) articular-sided SSP and/or ISP tendon tears, (3) subcortical humeral head cysts, (4) thickening of the posterior capsule and controversial laxity of the anterior capsule,[3,11,18,55] and (5) regional alterations in the glenoid version above the central equator and can be associated with anterior shoulder instability[11] (Figure 16).

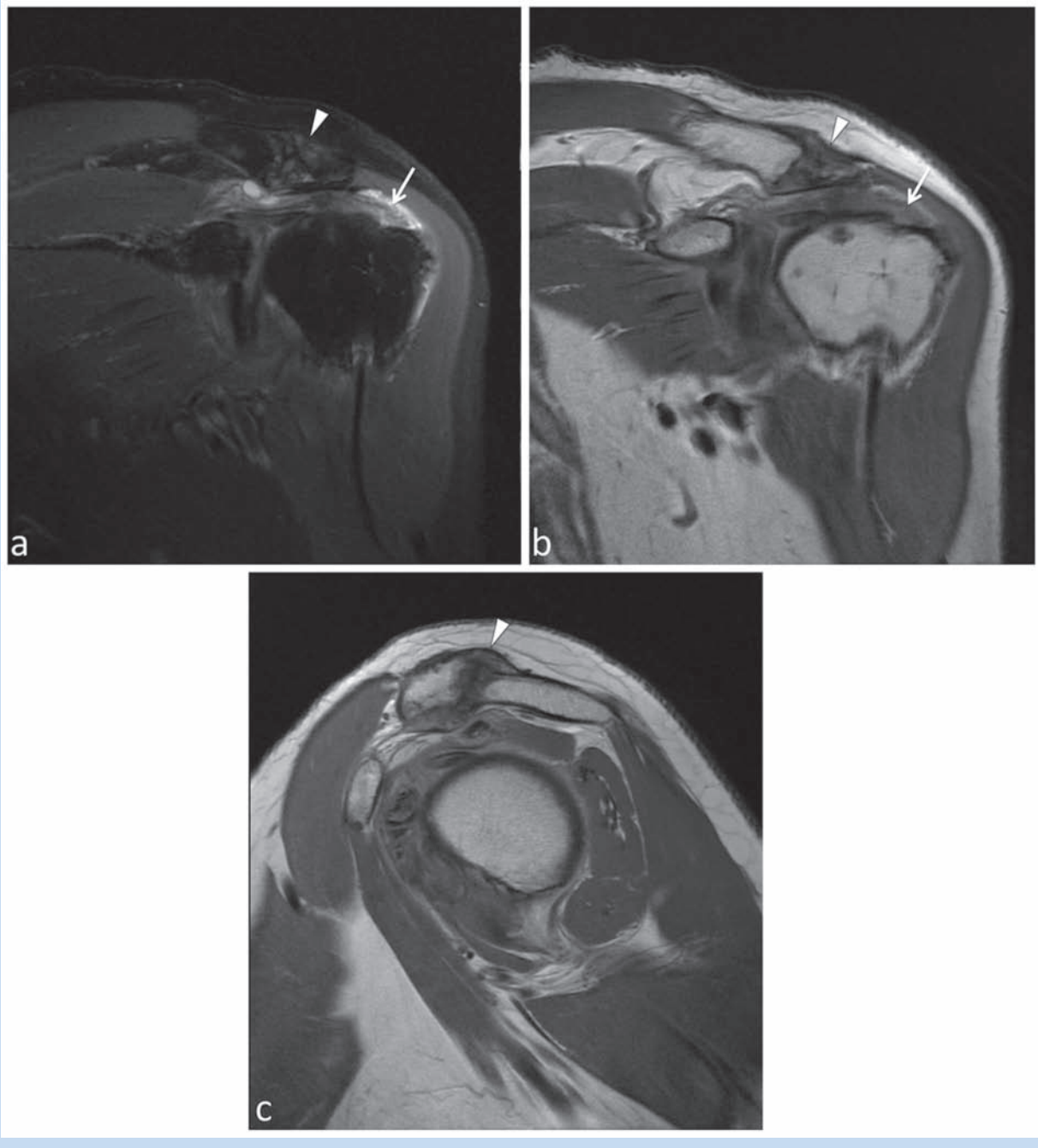

Figure 13. AC joint osteoarthritis (arrowhead) with subacromial impingement and bursal-sided SSP partial tear (arrow) in a 57-year-old patient are shown on oblique coronal (a) T2w FS FSE and (b) PDw FSE as well as on (c) oblique sagittal PDw FSE images. AC, acromioclavicular; SSP, supraspinatus; T2w FS FSE, T2-weighted fat-suppressed fast spin echo; PDw FSE, proton density–weighted fast spin echo.

Figure 14. Schematic illustration of the different acromion types, as described by Bigliani.[4]

SHOULDER IMPINGEMENT: PEARLS AND PITFALLS

- Impingement is mainly a clinical diagnosis; MRI may be helpful in defining anatomical alterations that lead to the clinical symptoms
- Impingement can be categorized as external (subacromial and subcoracoid) and internal
- Subacromial impingement can be caused by certain acromial morphologies, AC joint arthritis, os acromiale, and a hypertrophied coracoacromial ligament

CAPSULO-LIGAMENTOUS-LABRAL COMPLEX

Labrum

Anatomy, normal variations, and MR appearance. The labrum attaches at the glenoid rim to increase the glenoid surface, thus serving as an important stabilizer of the glenohumeral joint. It is a complex fibrocartilaginous structure with high individual anatomical variations.[44] A knowledge of the anatomical variants is crucial to differentiate from pathologies. Anatomical variants include (1) the sublabral recess or sulcus, (2) the sublabral foramen, and the (3) Buford complex[44] (Figure 12).

The superior labral recess/sulcus is a space beneath the superior glenoid and the biceps-labral complex, courses along the glenoid surface, and is classically located superiorly (between 11 and 1 o'clock positions of the glenoid surface)[44] (Figure 12b).

The sublabral foramen is a physiologic detachment of the anterosuperior labrum and is located in the anterosuperior quarter of the glenoid surface[44] (Figure 12c).

The Buford complex reflects an absent or markedly deficient anterior labrum with a thickened MGHL[44,64] (Figure 12d).

Diagnostic criteria for the normal anatomical variants of the labrum are: (1) their specific locations, (2) their smooth and tapering appearance, and (3) their course parallel to the glenoid surface.[44] When imaging the middle-aged or older athlete, however, note should be made that these anatomical variants are subject to fraying and degeneration, altering their signal characteristics and morphology on MRI. The MR appearance of the labrum usually is triangular in shape and of low signal intensity on all pulse sequences. Alteration in shape and signal intensity, however, is not diagnostic of labral pathology, and a knowledge of anatomical variants and senescent changes is important to ensure reliable diagnosis.[65]

Labral pathologies. General criteria for labral tears are: (1) a hyperintense lesion within the labrum, not at the typical location for normal anatomical variants; (2) an irregularity in morphology; and (3) an abnormal course of the labral lesion away from the glenoidal surface (toward lateral).[44]

A superior labrum anterior and posterior lesion (SLAP) is a lesion of the superior labrum that may affect the biceps anchor. Four different SLAP lesions were first described by Snyder[51]; newer classifications have increased this to 10 different types[32,34] (Table 3 and Figure 17).

The Bankart lesion is an anteroinferior labrum tear with associated disruption of the scapular attachment of the capsule. It is further classified as bony if an osseous glenoid defect is present[1] (Figures 18 and 19d).

The Perthes lesion is an often nondisplaced or minimally displaced labral tear in which the scapular attachment of the capsule remains intact[41,46] (Figures 18 and 20c).

The anterior labroligamentous periosteal sleeve avulsion (ALPSA) lesion is a labrum lesion in which the labrum is displaced inferomedially, tethered by the periosteal stripping at the capsule[37] (Figures 18 and 20a).

The glenolabral articular disruption (GLAD) lesion is closely related to the Perthes lesion but has an associated articular cartilage injury[38] (Figures 18 and 20b).

Paralabral cysts or ganglions are associated with labral tears and are detected as round or multiseptated fluid-filled masses on fluid-sensitive MR sequences.[46] Paralabral cysts can become very large and may lead to nerve compression at the spinoglenoid notch, suprascapular notch, or the quadrilateral space (Figure 17).

Glenohumeral Ligaments and Capsule

Anatomy, normal variants, and MR appearance. The humeral capsule is strengthened by 3 glenohumeral ligaments that are best evaluated in the axial and oblique coronal planes: the superior glenohumeral ligament (SGHL), the middle glenohumeral ligament (MGHL), and the inferior glenohumeral ligament (IGHL), with the IGHL as the most important and the SGHL as the least important ligament component to impart the overall stability of the glenohumeral joint[2] (Figure 12).

The MGHL is the most variable ligament as it can be completely absent, appear as thick cordlike ligament, or as part of the Buford complex (absent anterior labrum with a thickened MGHL)[45] (Figure 12). The IGHL is composed of a reciprocal anterior and posterior band within the axillary pouch.

Pathologies of the glenohumeral ligaments. Humeral avulsion of glenohumeral ligaments (HAGL) can result in glenohumeral instability. An HAGL should be ruled out, particularly in

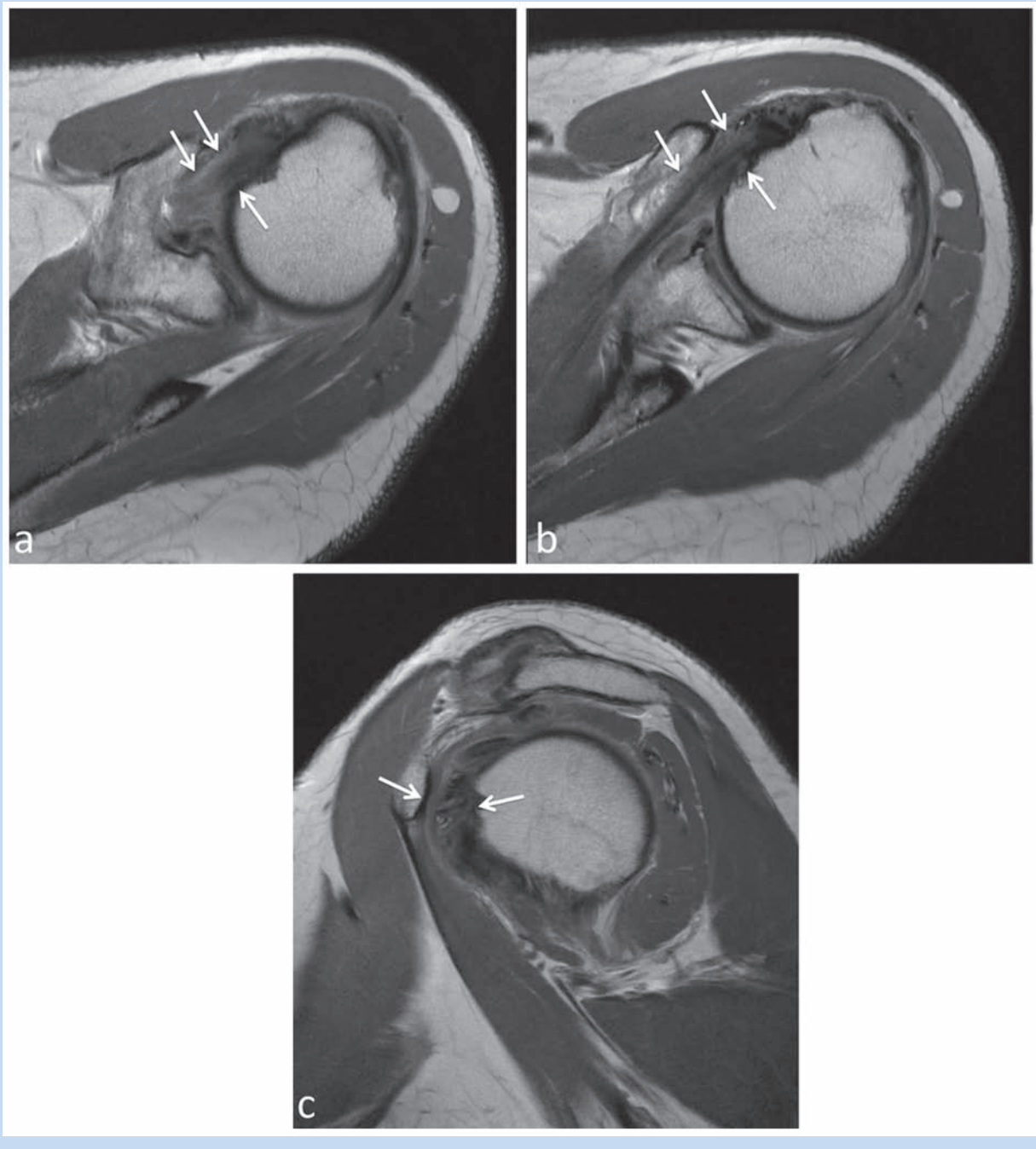

Figure 15. Subcoracoid impingement with narrowing of the subcoracoid space (arrows) and resultant SSC tendinopathy (arrows) in a 67-year-old patient, shown on (a and b) axial PDw FSE and (c) oblique sagittal PDw FSE images. SSC, subscapularis; PDw FSE, proton density–weighted fast spin echo.

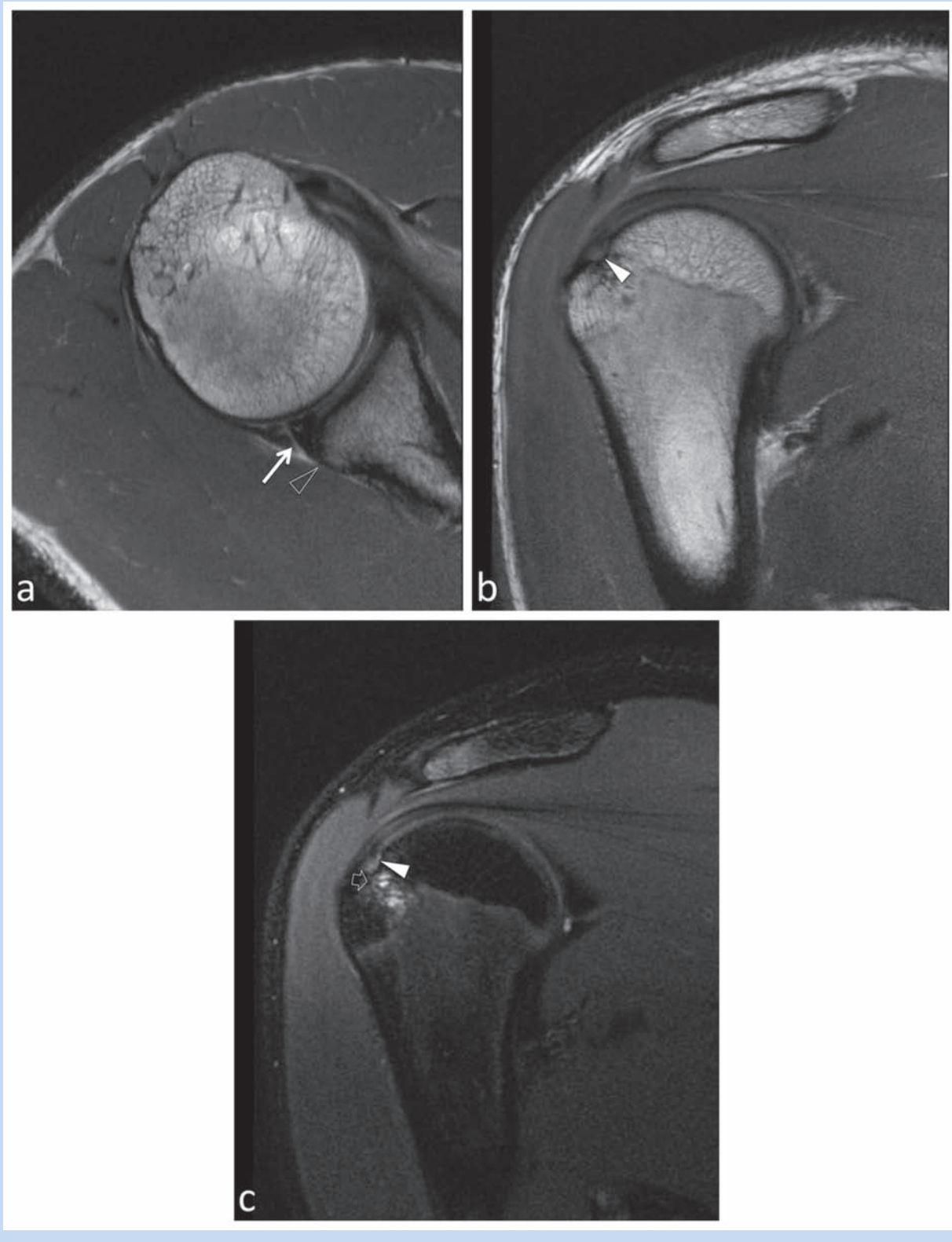

Figure 16. A 20-year-old patient with internal impingement. (a) shows a posterior labral tear, remodeling of the posterior gleniod with regional alteration in the glenoid version, and a focal Bennett lesion (open arrowhead). Oblique coronal (b) PDw FSE and (c) T2w FS FSE images show an articular-sided partial ISP tear (arrowheads) with associated humeral head cysts (open arrow). PDw FSE, proton density–weighted fast spin echo; T2w FS FSE, T2-weighted fat-suppressed fast spin echo; ISP, infraspinatus.

Table 3. The different types of SLAP lesions.[32,34,51]

SLAP Lesion Type	Pathologic Findings
Type I	Degenerative change of the superior labrum
Type II	Tear with biceps anchor detachment
Type III	Bucket-handle tear of the superior labrum with an intact biceps anchor
Type IV	Bucket-handle tear of the superior labrum with involvement of the biceps anchor and biceps tendon
Type V	Extension of a Bankart lesion with involvement of the superior labrum and biceps anchor or a SLAP lesion with anterior inferior extension
Type VI	Anterior or posterior flap tear similar to SLAP Type IV or III with a bucket-handle component
Type VII	Extension of a SLAP lesion into the glenohumeral ligament
Type VIII	Extension of a SLAP lesion into the posterior labrum and further abnormalities
Type IX	Circumferential labral detachment
Type X	Extension to the rotator cuff interval and articular-sided abnormalities

SLAP, superior labrum anterior and posterior lesion.

patients who have anterior instability after a violent injury without a Bankart lesion.[5] A J-shape axillary pouch, seen on oblique coronal MR images, has been described as a sign for a HAGL lesion (Figure 21), as normally the axillary pouch should show a U-shape with distension of the joint (with joint fluid or intra-articular CM application).[6] HAGL lesions may require a modified (open) surgical treatment technique. Rarely, HAGL lesions may coexist with Bankart lesions.

Bony humeral avulsion of glenohumeral ligaments (BHAGL) is a variant of the HAGL that is associated with a bony avulsion at the humeral attachment (Figure 22).

Glenohumeral Instability

MR findings with anterior instability. The most common injuries with anterior shoulder instability are a Hill Sachs lesion[21] and a Bankart lesion[1] (Figure 19).

The Hill Sachs lesion is a compression fracture at the posterosuperior aspect of the humeral head, best evaluated in the axial plane, at or above the level as the coracoid process. Associated bone marrow edema is seen on fluid-sensitive sequences (T2w FS or STIR) (Figure 19).

The Bankart lesion is an anterior inferior labrum tear with associated disruption of the joint capsule (Figures 18 and 19d).[5]

Posterior instability. MR findings with posterior instability:

The reverse Hill Sachs lesion represents a compression fracture of the anterosuperior humeral head (Figure 23).

The reverse Bankart lesion is similar to the classic Bankart lesion but at the posterior labrum (Figure 18).

The posterior labrocapsular periosteal sleeve avulsion (POLPSA), reverse Perthes, and the reverse GLAD lesion correspond to the ALPSA and GLAD lesion, respectively, but at the posterior labrum (Figure 18).

A reverse HAGL/BHAGL lesion corresponds to a rupture of the posterior band of the IGHL with or without a humeral avulsion fracture.

The Bennett lesion is ossification of the posterior capsule, sometimes secondary to posterior subluxation[10] (Figure 16).

Rotator cuff lesion seems to be more often associated with posterior shoulder dislocation than previously thought.[47]

Glenoid dysplasia should always be excluded particularly in a patient with recurrent shoulder instability (Figure 24). A recent study concludes that the glenoid morphology may even be more important than the glenoid retroversion in case of instability.[22]

GLENOHUMERAL INSTABILITY: PEARLS AND PITFALLS

- Hill Sachs lesion is best detected on the axial plane on the posterosuperior aspect of the humeral head, at the level of the coracoid process or above
- Normal flattening of the posterior humeral head should not be mistaken for a Hill Sachs lesion
- A HAGL lesion can result in anterior instability and should be ruled out in the setting of anterior dislocation without a Bankart lesion
- Findings associated with posterior instability include a reverse Bankart lesion and a reverse Hill Sachs lesion
- The circle concept dictates that forces leading to damage due to impaction or compression on one side of the joint may result in stretch or avulsion to structures on the opposite of the joint

Adhesive Capsulitis or "Frozen Shoulder"

MR characteristic findings include (1) complete obliteration of the rotator cuff interval, (2) thickening of the CHL (> 4 mm), and (3) a thickened joint capsule in the rotator cuff interval (> 7 mm), with decreasing specificity but increasing sensitivity

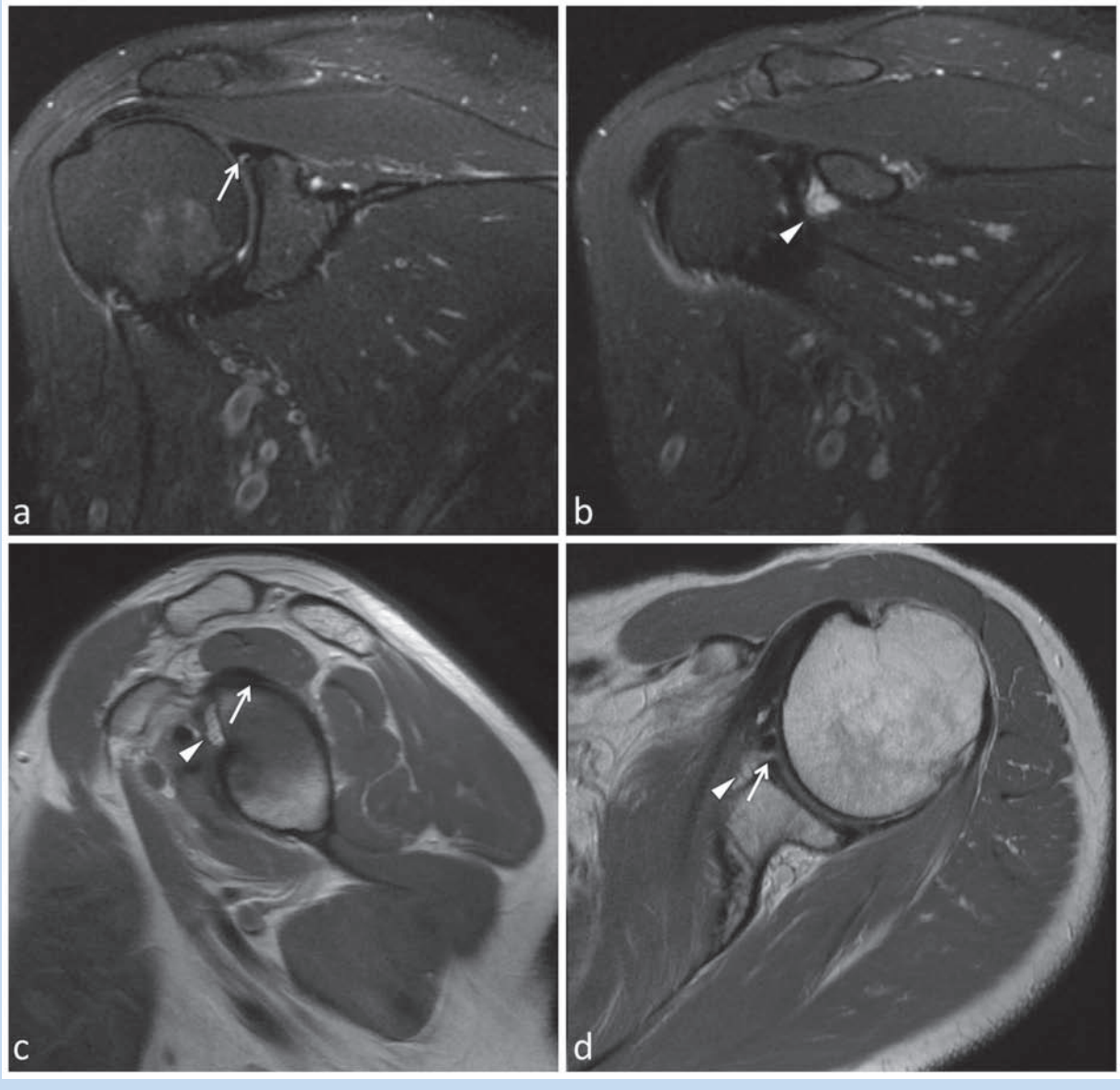

Figure 17. SLAP lesion (arrow) with ganglion formation (arrowhead) in a 47-year-old patient shown on (a and b) oblique coronal T2w FS FSE, (c) oblique sagittal, and (d) axial PDw FSE images. SLAP, superior labrum anterior and posterior lesion; T2w FS FSE, T2-weighted fat-suppressed fast spin echo; PDw FSE, proton density–weighted fast spin echo.

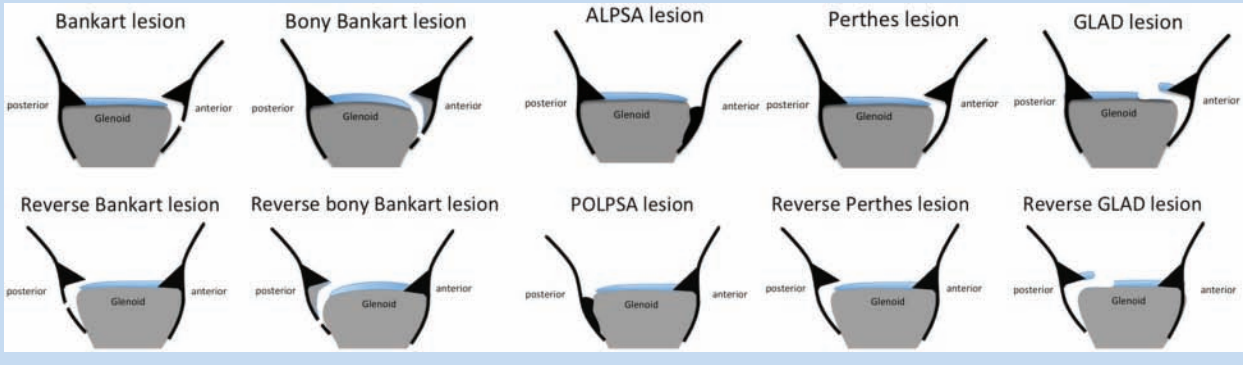

Figure 18. Schematic illustration of the Bankart lesion and Bankart lesion variations.

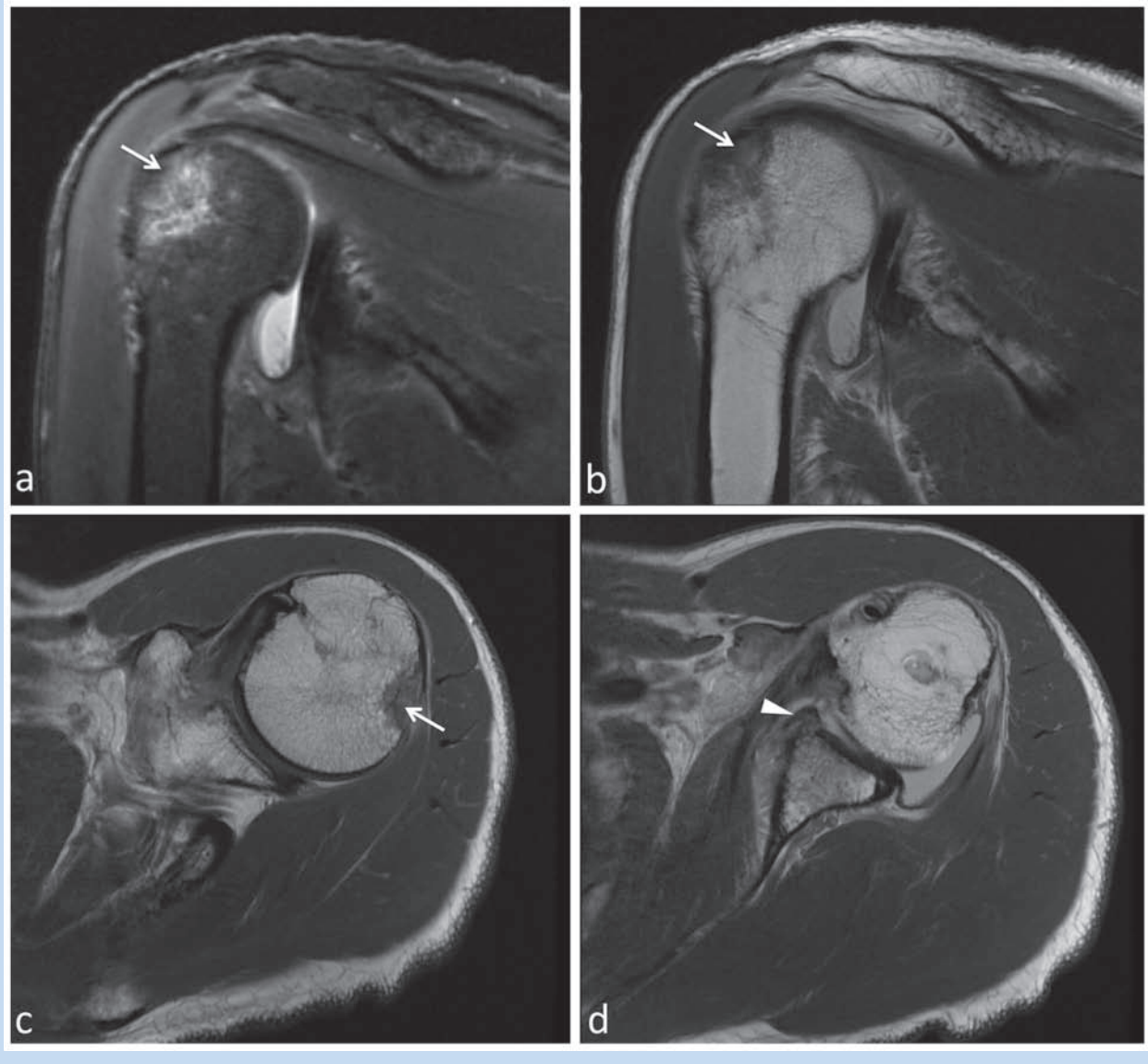

Figure 19. Anterior shoulder instability in a 58-year-old patient. (a) Oblique coronal T2w FS FSE image and (b) oblique coronal PDw FSE image show bone marrow edema at the superior aspect of the humeral head indicating a Hill Sachs lesion (arrow). (c and d) Axial PDw FSE better visualizes the Hill Sachs lesion (arrow) at the posterosuperior humeral head (note the coracoid process to correlate the height) and a Bankart lesion (arrowhead). T2w FS FSE, T2-weighted fat-suppressed fast spin echo; PDw FSE, proton density–weighted fast spin echo.

from (1) to (3), described by Menigiardi et al[33,35] (Figure 25). The inferior joint recess often appears indistinct from the adjacent muscle due to the increased mobility of water in the tissue and the presence of extracapsular soft tissue edema indicating autodecompression of the capsule into the adjacent tissues that may help differentiate this stage from the others[52] (Figure 26). In the early stage, the capsule is not quite as thick and there is often some synovial debris in the dependent portion of the axillary pouch, although significant differences between the stages were not shown.[52]

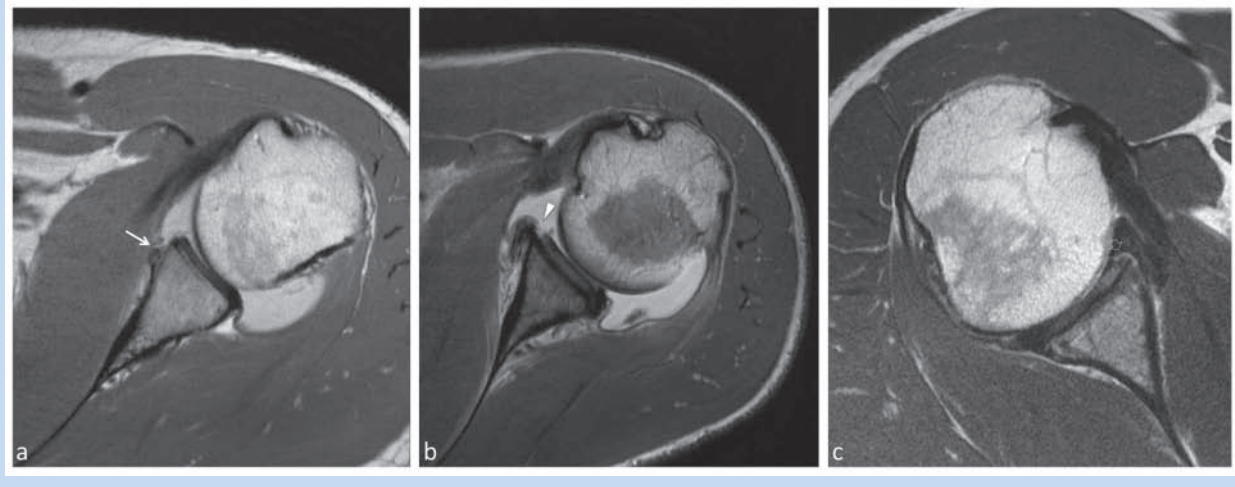

Figure 20. Axial PDw FSE images show (a) an ALPSA lesion (arrow) in a 26-year-old patient, (b) a GLAD lesion in a 29-year-old patient (arrowhead), and (c) a Perthes lesion in a 35-year-old patient. PDw FSE, proton density–weighted fast spin echo; ALPSA, anterior labroligamentous periosteal sleeve avulsion; GLAD, glenolabral articular disruption.

Figure 21. Coronal oblique (a) T2w FS FSE and (b) PDw FSE images show an HAGL lesion of the IGHL with the classic "J-sign" (arrow) in a 30-year-old patient. T2w FS FSE, T2-weighted fat-suppressed fast spin echo; PDw FSE, proton density–weighted fast spin echo; HAGL, humeral avulsion of glenohumeral ligaments; IGHL, inferior glenohumeral ligament.

ADHESIVE CAPSULITIS: PEARLS AND PITFALLS

- Mainly a clinical diagnosis, presenting with pain and decreased range of motion
- MR findings: Complete obliteration of the rotator cuff interval, thickening of the CHL, and thickening and hyperintensity of the joint capsule, particularly in the axillary recess and gadolinium-enhancement of the capsule
- The clinical described stage II (inflammatory stage) may be identified on MR by its hyperintense signal around the capsule compared with other stages

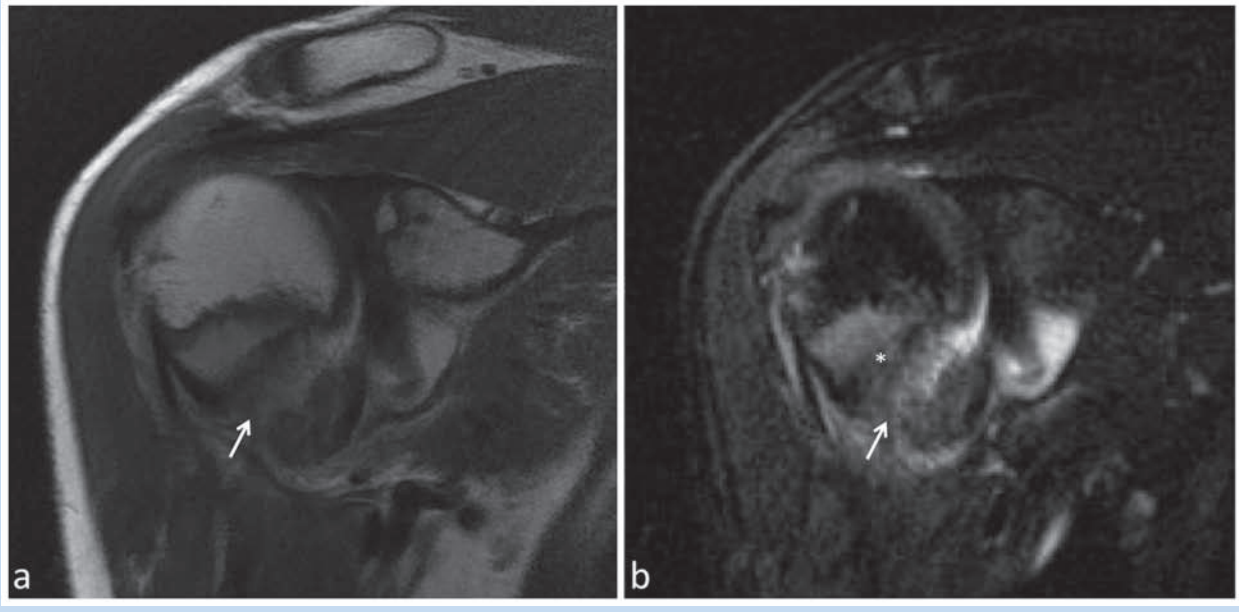

Figure 22. Bony HAGL in a 13-year-old boy, shown on oblique coronal (a) PDw FSE and (b) T2w FS FSE images. Note bone marrow edema at the humeral neck (*). HAGL, humeral avulsion of glenohumeral ligaments; PDw FSE, proton density–weighted fast spin echo; T2w FS FSE, T2-weighted fat-suppressed fast spin echo.

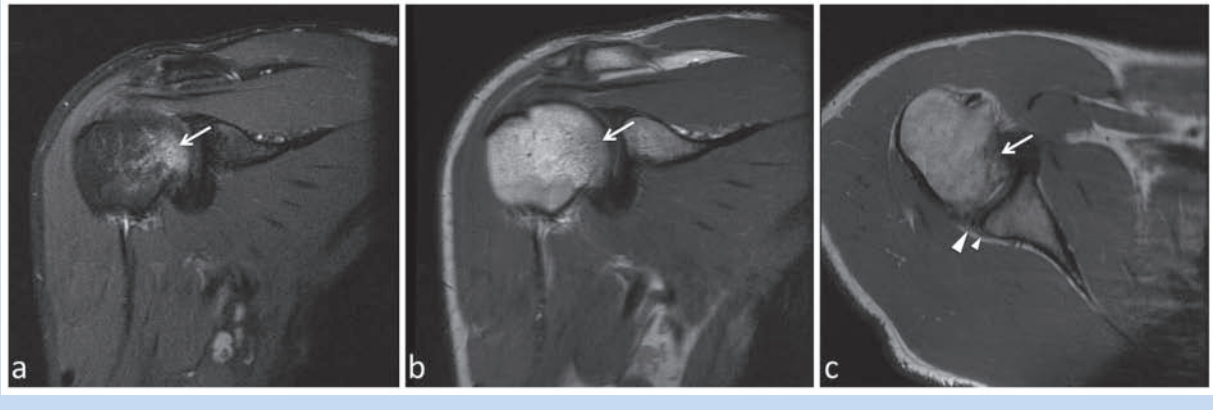

Figure 23. Posterior instability in a 23-year-old patient. Oblique coronal (a) T2w FS FSE and (b) PDw FSE images show bone marrow edema (arrow). (c) Axial PDw FSE image shows the corresponding reverse Hill Sachs lesion anterosuperior at the humeral head (arrow) and a posterior labral tear (large arrowhead) with stripping of the posterior capsule from the scapula (small arrowhead). T2w FS FSE, T2-weighted fat-suppressed fast spin echo; PDw FSE, proton density–weighted fast spin echo.

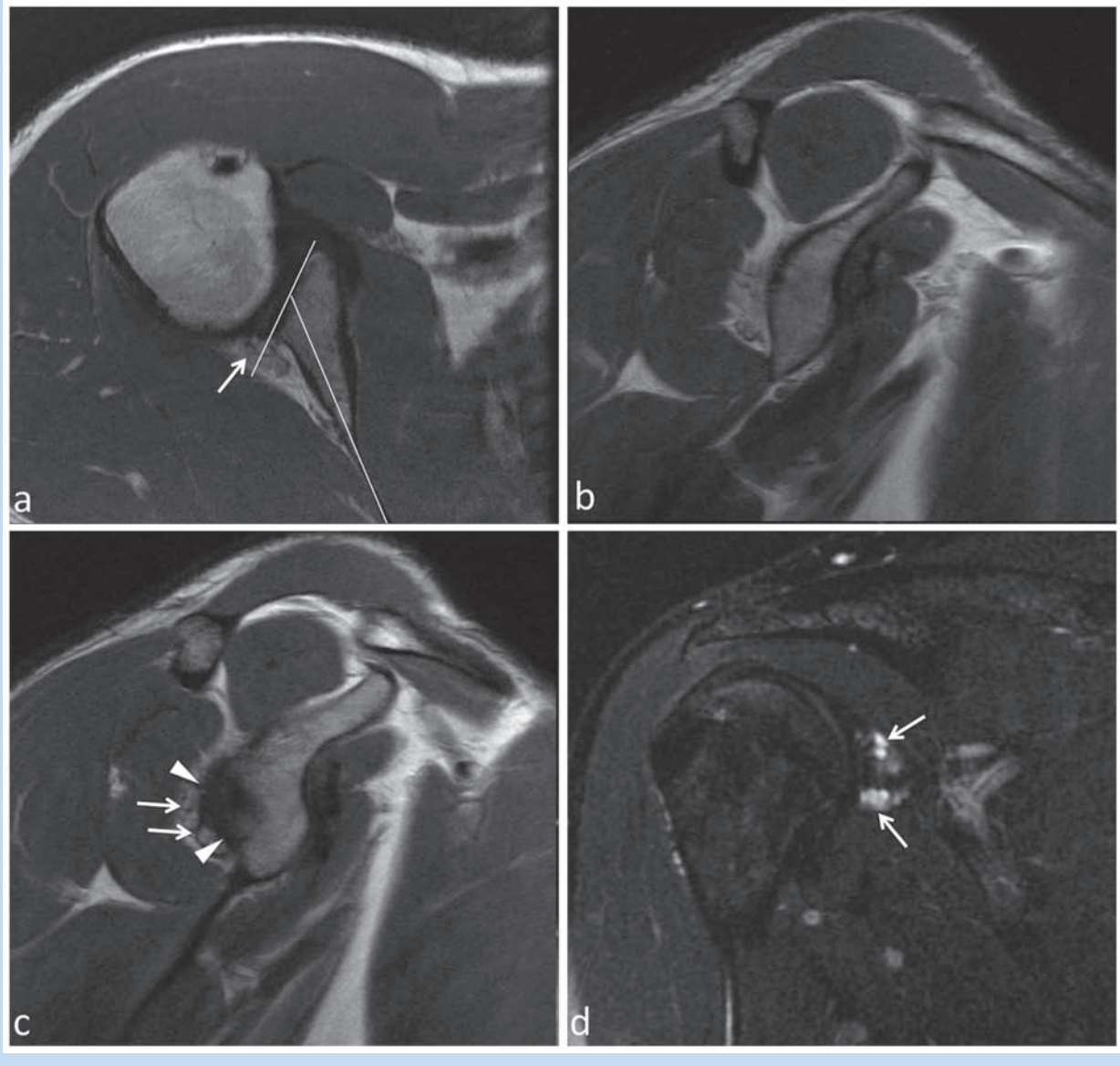

Figure 24. Glenoid dysplasia in a 19-year-old patient with recurrent shoulder instability. (a) An exaggerated retroversion of the glenoid surface (42° retroversion) and paralabral ganglia (arrow). (b and c) The oblique sagittal PDw FSE images show a hypoplastic glenoid morphology with hypertrophied posterior labrum (arrowheads) and ganglia formation (arrows). (d) Coronal T2w FS FSE image better visualizes the numerous, fluid-containing intralabral ganglia (arrows). PDw FSE, proton density–weighted fast spin echo; T2w FS FSE, T2-weighted fat-suppressed fast spin echo.

CARTILAGE AND OSSEOUS STRUCTURES

Articular Cartilage

Normal anatomy and MR appearance. The cartilage covering the humeral head and glenoid is best evaluated using the PDw sequence in the oblique coronal and axial planes. Normal cartilage usually appears of intermediate signal intensity on PDw sequences because of its water and extracellular matrix content[40] (Figure 27). The cartilage is generally thin, particularly at the glenoid surface, and its assessment remains challenging in MRI.

Pathologies of the articular cartilage. Chondral defects can be characterized by location (using a clock facing the glenoid surface), extent, depth (superficial, > 50% of cartilage depth involved, exposed subchondral bone), presence of associated

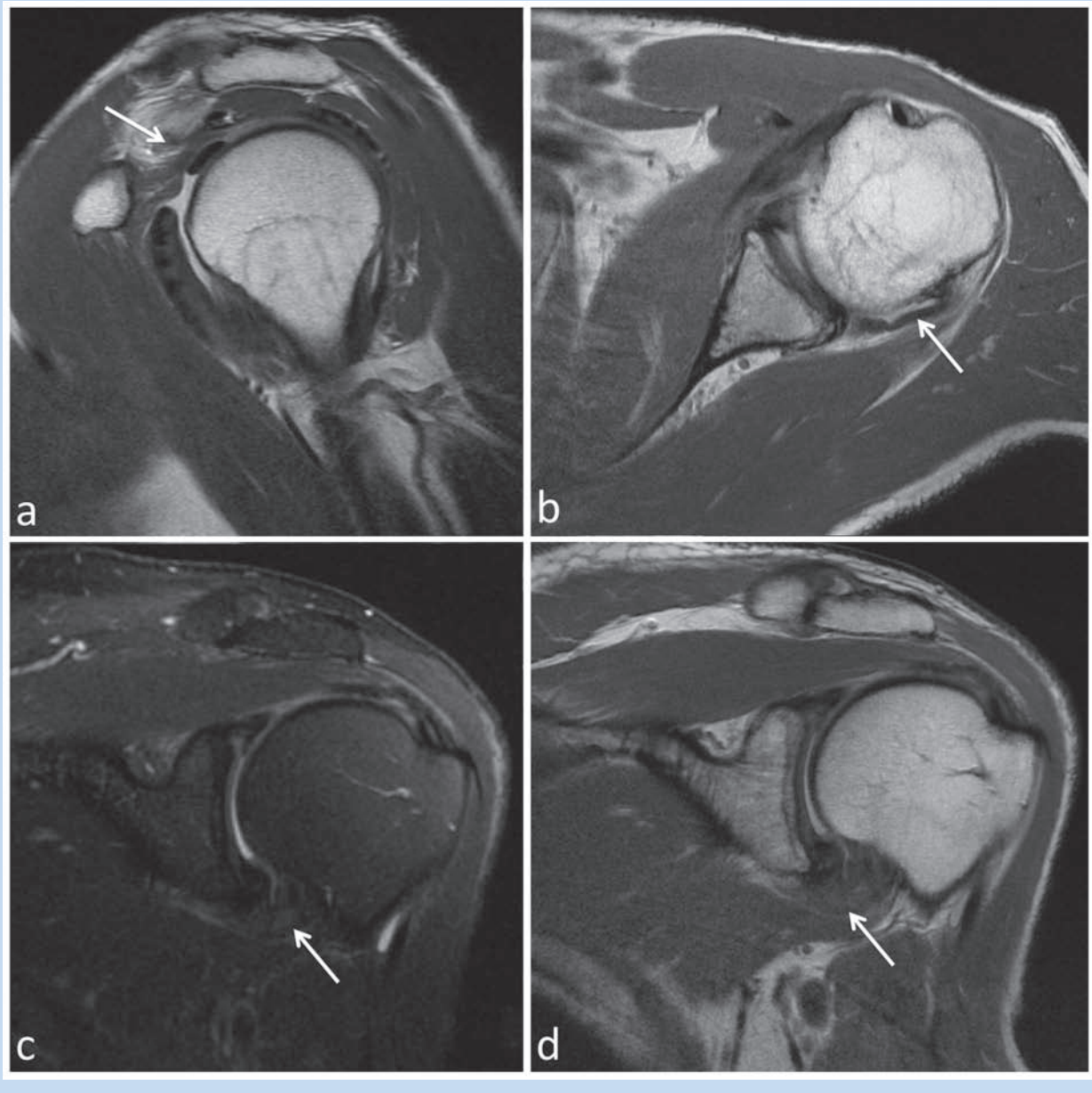

Figure 25. Adhesive capsulitis in a 59-year-old patient. (a) Oblique sagittal PDw FSE image shows obilteration of the rotator cuff interval (arrow) by thickening of the joint capsule and thickening of the coracohumeral and glenohumeral ligament. (b) Axial PDw FSE images show synovitis and thickening of the joint capsule anterior and posterior (arrow). Oblique coronal (c) T2w FS FSE and (d) PDw FSE images show thickening of the axillary recess capsule. PDw FSE, proton density–weighted fast spin echo; T2w FS FSE, T2-weighted fat-suppressed fast spin echo.

subchondral bone marrow edema, and/or associated loose intra-articular bodies (Figure 28).

Osseos structures. All the osseous structures should be evaluated for bone marrow edema by using the T2w sequences and for possible fracture lines using the T1w or PDw sequences. Fat suppression will increase the dynamic contrast range, making marrow edema much more conspicuous (Figures 19a and 23a).

The glenoid morphology is important in case of recurrent shoulder instability. A normal glenoid is usually slightly retroverted (mean, 4°).[44] In case of glenoid dysplasia, a biconcave glenoid morphology, a hypoplasia of the posteroinferior glenoid rim associated

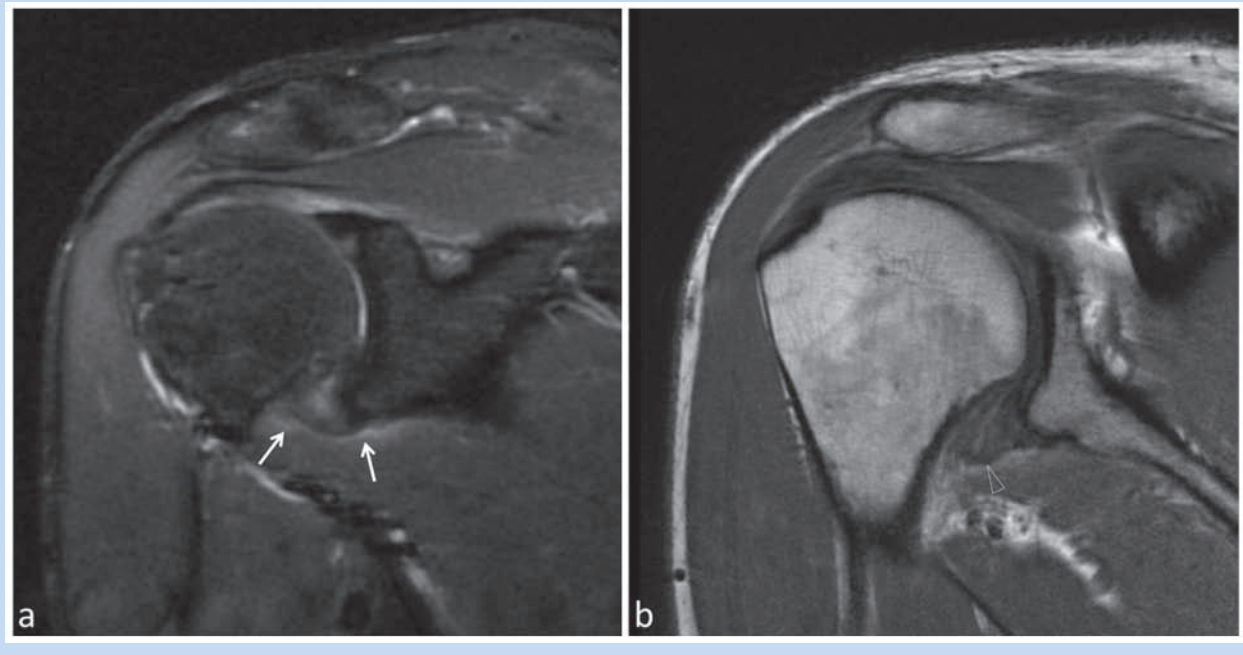

Figure 26. Oblique coronal (a) T2w FS FSE and (b) PDw FSE images show a thickened glenohumeral joint capsule with focal edema corresponding to the inflammatory, stage II of adhesive capsulitis in a 49-year-old patient. T2w FS FSE, T2-weighted fat-suppressed fast spin echo; PDw FSE, proton density–weighted fast spin echo.

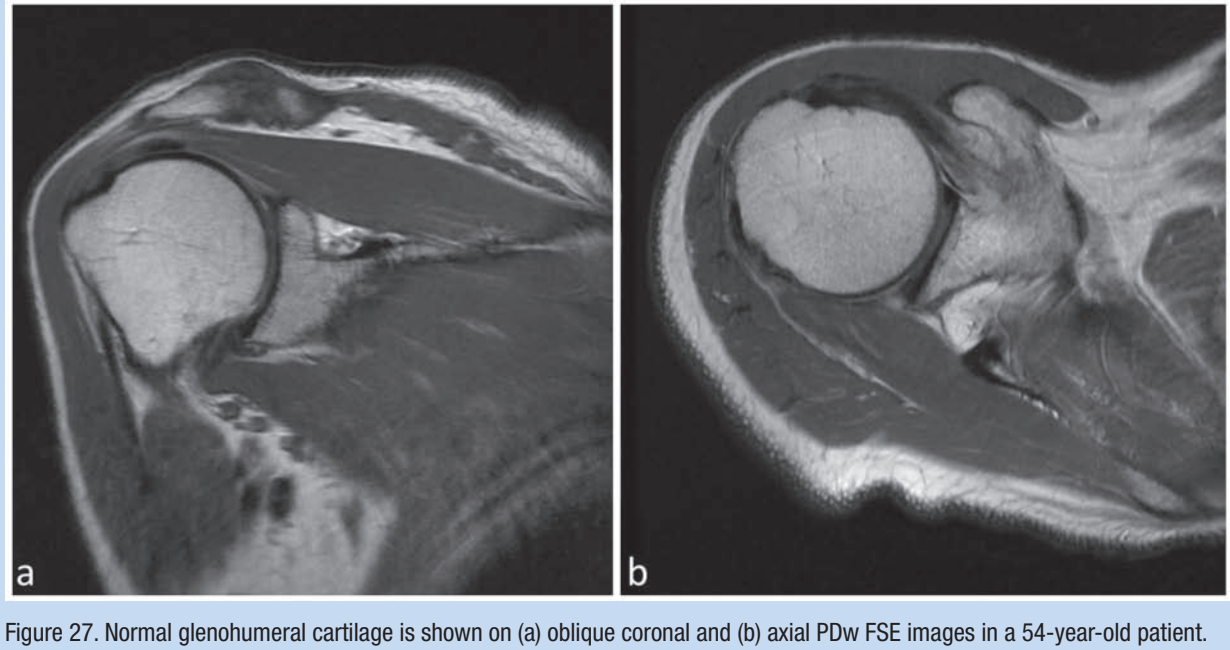

Figure 27. Normal glenohumeral cartilage is shown on (a) oblique coronal and (b) axial PDw FSE images in a 54-year-old patient. PDw FSE, proton density–weighted fast spin echo.

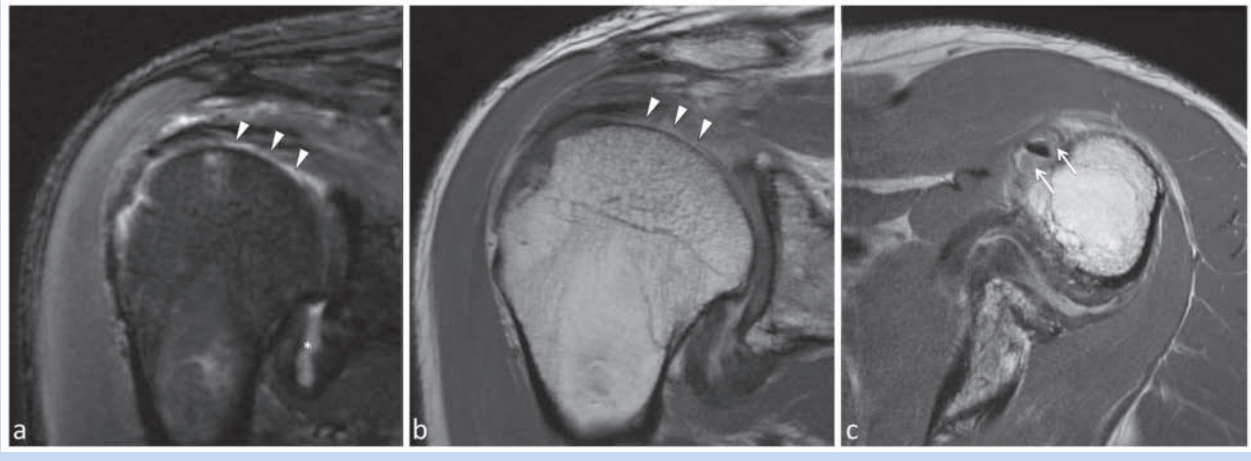

Figure 28. Extensive chondral loss over the humeral head (arrowheads) with debris within the axillary recess (*) and biceps tendon sheath (arrows) in a 51-year-old patient with OA, demonstrated on oblique coronal (a) T2w FS FSE and (b) PDw FSE as well as (c) axial PDw FSE images. OA, osteoarthritis; T2w FS FSE, T2-weighted fat-suppressed fast spin echo; PDw FSE, proton density–weighted fast spin echo.

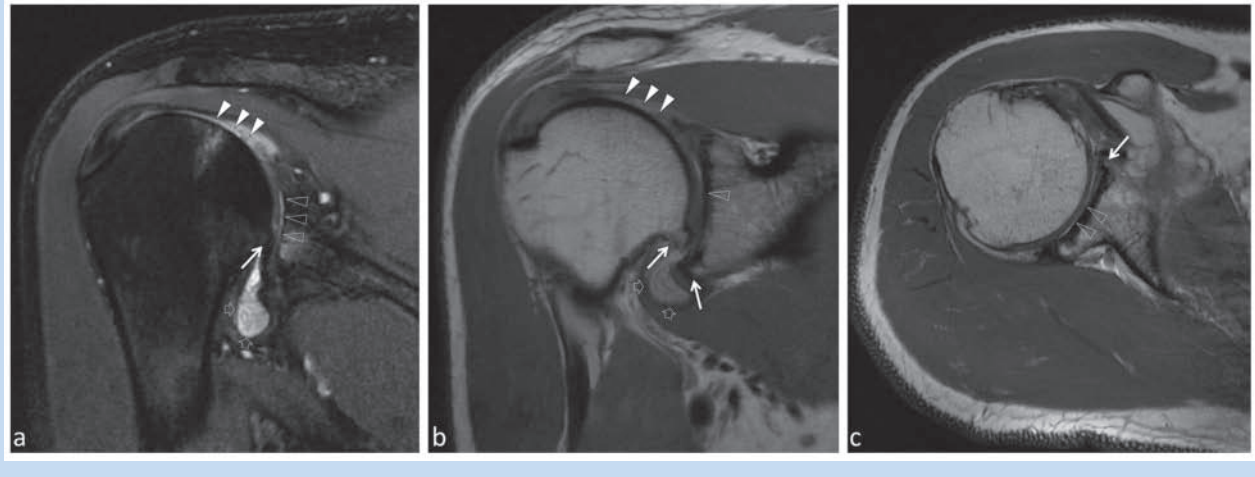

Figure 29. Severe OA in a 53-year-old patient. Oblique coronal (a) T2w FS FSE and (b) PDw FSE images show osteophyte formation at the humeral head and glenoid inferiorly (arrows), large chondral loss with exposed bone and subchondral cyst formation over the humeral head (arrowheads) and in the center of the glenoid (open arrowheads) with resultant chondral debris visible within the axillary recess (open arrows). (c) Axial PDw FSE image better visualizes the large chondral loss at the glenoid surface with exposed bone (open arrowheads). Note the osteophyte at the glenoid anteriorly (arrow). OA, osteoarthritis; T2w FS FSE, T2-weighted fat-suppressed fast spin echo; PDw FSE, proton density–weighted fast spin echo.

with a hypertrophied posterior labrum, and a pronounced glenoid retroversion (> 5°) may be found[22,44,62] (Figure 24).

Glenohumeral and Acromioclavicular Joint Osteoarthritis

Osteoarthritis (OA) may be degenerative or secondary to trauma, infection, metabolic, or congenital disorders. MR findings of osteoarthritis include (1) joint narrowing, (2) subchondral sclerosis, (3) osteophyte formation, (4) subchondral cysts, (5) chondral erosions, and (6) synovitis (Figures 28 and 29). Recognition of OA in the middle-aged athlete is important and may co-exist with lesions of the rotator cuff, biceps, and superior labrum.[26]

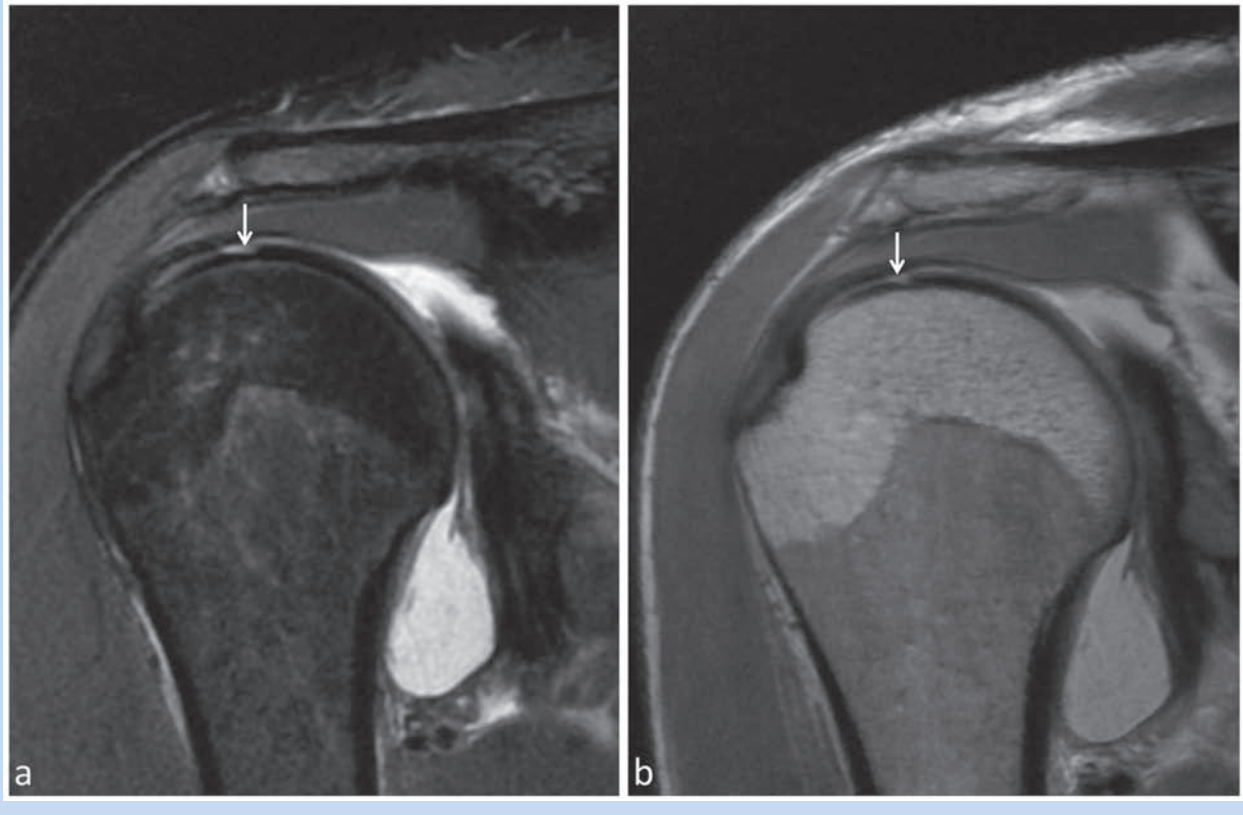

Figure 30. Early chondral loss over the humeral head (arrows) in a 29-year-old patient as an early manifestation of OA, shown in oblique coronal (a) T2w FS FSE and (b) PDw FSE images. OA, osteoarthritis; T2w FS FSE, T2-weighted fat-suppressed fast spin echo; PDw FSE, proton density–weighted fast spin echo.

Early changes include osteophyte formation and early cartilage loss. The earliest osteophyte formation has been described at the articular margin of the humeral head and at the line of attachment of the labrum to the glenoid[26] (Figure 29).

Early cartilage loss is typically found over the humeral head and noted on the oblique coronal images (Figure 30) and later in the center of the glenoid fossa.[26,36] Loose intra-articular bodies may occur with fragmentation of the osteochondral surfaces and are often found in the superior recess of the subscapularis bursa, located inferior to the coracoid on the oblique sagittal images, in the axillary recesses and the biceps tendon sheath[36] (Figure 28).

Glenohumeral joint narrowing seems to be a relatively late manifestation of glenohumeral OA.[26]

Static posterior humeral head subluxation is often associated with OA and may be seen in young adults at the first stage of primary glenohumeral OA.[16,59]

The synovitis and bone changes associated with OA serve as significant pain generators that limit functional recovery following treatment aimed only at the tendons and labrum.

Acromioclavicular (AC) joint osteoarthritis is defined by capsular hypertrophy, osteophyte formation, bony erosion, and bone marrow edema (Figure 13) and can cause subacromial impingement.

OSTEOARTHRITIS: PEARLS AND PITFALLS

- OA is associated with joint narrowing, synovitis, subchondral sclerosis, osteophyte formation, subchondral cysts, and chondral erosions
- Early OA is associated with cartilage loss over the humeral head
- Loose intra-articular osteochondral bodies may be found in the axillary pouch, superior recess of the subscapularis bursa, and biceps tendon sheath
- Posterior humeral head subluxation may be associated with OA

ACKNOWLEDGMENT

The authors thank the MR department of the Hospital for Special Surgery for providing the MR images used in this article.

REFERENCES

1. Bankart ASB. Recurrent or habitual dislocation of the shoulder joint. *Nebr Med J.* 1923;2:1132-1133.
2. Beltran J, Rosenberg ZS, Chandnani VP, Cuomo F, Beltran S, Rokito A. Glenohumeral instability: evaluation with MR arthrography. *Radiographics.* 1997;17(3):657-673.
3. Beltran LS, Nikac V, Beltran J. Internal impingement syndromes. *Magn Reson Imaging Clin N Am.* 2012;20(2):201-211, ix-x.
4. Bigliani LU, Ticker JB, Flatow EL, Soslowsky LJ, Mow VC. Relationship of acromial architecture and diseases of the rotator cuff [in German]. *Orthopade.* 1991;20(5):302-309.
5. Bokor DJ, Conboy VB, Olson C. Anterior instability of the glenohumeral joint with humeral avulsion of the glenohumeral ligament. A review of 41 cases. *J Bone Joint Surg Br.* 1999;81(1):93-96.
6. Carlson CL. The "J" sign. *Radiology.* 2004;232(3):725-726.
7. Curtis AS, Burbank KM, Tierney JJ, Scheller AD, Curran AR. The insertional footprint of the rotator cuff: an anatomic study. *Arthroscopy.* 2006;22(6):609.e1.
8. Davis SJ, Teresi LM, Bradley WG, Ressler JA, Eto RT. Effect of arm rotation on MR imaging of the rotator cuff. *Radiology.* 1991;181(1):265-268.
9. de Jesus JO, Parker L, Frangos AJ, Nazarian LN. Accuracy of MRI, MR arthrography, and ultrasound in the diagnosis of rotator cuff tears: a meta-analysis. *Am J Roentgenol.* 2009;192(6):1701-1707.
10. De Maeseneer M, Jaovisidha S, Jacobson JA, et al. The Bennett lesion of the shoulder. *J Comput Assist Tomogr.* 1998;22(1):31-34.
11. Drakos MC, Rudzki JR, Allen AA, Potter HG, Altchek DW. Internal impingement of the shoulder in the overhead athlete. *J Bone Joint Surg Am.* 2009;91(11):2719-2728.
12. Ellman H. Diagnosis and treatment of incomplete rotator cuff tears. *Clin Orthop Relat Res.* 1990;254:64-74.
13. Erickson SJ, Cox IH, Hyde JS, Carrera GF, Strandt JA, Estkowski LD. Effect of tendon orientation on MR imaging signal intensity: a manifestation of the "magic angle" phenomenon. *Radiology.* 1991;181(2):389-392.
14. Fuchs B, Weishaupt D, Zanetti M, Hodler J, Gerber C. Fatty degeneration of the muscles of the rotator cuff: assessment by computed tomography versus magnetic resonance imaging. *J Shoulder Elbow Surg.* 1999;8(6):599-605.
15. Garofalo R, Conti M, Massazza G, Cesari E, Vinci E, Castagna A. Subcoracoid impingement syndrome: a painful shoulder condition related to different pathologic factors. *Musculoskelet Surg.* 2011;95(suppl 1):S25-S29.
16. Gerber C, Costouros JG, Sukthankar A, Fucentese SF. Static posterior humeral head subluxation and total shoulder arthroplasty. *J Shoulder Elbow Surg.* 2009;18(4):505-510.
17. Gerber C, Krushell RJ. Isolated rupture of the tendon of the subscapularis muscle. Clinical features in 16 cases. *J Bone Joint Surg Br.* 1991;73(3):389-394.
18. Giaroli EL, Major NM, Higgins LD. MRI of internal impingement of the shoulder. *Am J Roentgenol.* 2005;185(4):925-929.
19. Gleason PD, Beall DP, Sanders TG, et al. The transverse humeral ligament: a separate anatomical structure or a continuation of the osseous attachment of the rotator cuff? *Am J Sports Med.* 2006;34(1):72-77.
20. Goutallier D, Postel JM, Bernageau J, Lavau L, Voisin MC. Fatty muscle degeneration in cuff ruptures. Pre- and postoperative evaluation by CT scan. *Clin Orthop Relat Res.* 1994;304:78-83.
21. Hill HA, Sachs MD. The groove defect of the humeral head: a frequently unrecognized complication of dislocations of the shoulder joint. *Radiology.* 1940;35:690-700.
22. Hoenecke HR, Tibor LM, D'Lima DD. Glenoid morphology rather than version predicts humeral subluxation: a different perspective on the glenoid in total shoulder arthroplasty. *J Shoulder Elbow Surg.* 2012;21(9):1136-1141.
23. Hurt G, Baker CL. Calcific tendinitis of the shoulder. *Orthop Clin North Am.* 2003;34(4):567-575.
24. Jung J-Y, Jee W-H, Chun HJ, Ahn MI, Kim Y-S. Magnetic resonance arthrography including ABER view in diagnosing partial-thickness tears of the rotator cuff: accuracy, and inter- and intra-observer agreements. *Acta Radiol.* 2010;51(2):194-201.
25. Kassarjian A, Bencardino JT, Palmer WE. MR imaging of the rotator cuff. *Radiol Clin North Am.* 2006;44(4):503-523, vii-viii.
26. Kerr R, Resnick D, Pineda C, Haghighi P. Osteoarthritis of the glenohumeral joint: a radiologic-pathologic study. *Am J Roentgenol.* 1985;144(5):967-972.
27. Khan KM, Cook JL, Bonar F, Harcourt P, Astrom M. Histopathology of common tendinopathies. Update and implications for clinical management. *Sports Med.* 1999;27(6):393-408.
28. Kjellin I, Ho CP, Cervilla V, et al. Alterations in the supraspinatus tendon at MR imaging: correlation with histopathologic findings in cadavers. *Radiology.* 1991;181(3):837-841.
29. Lee SY, Lee JK. Horizontal component of partial-thickness tears of rotator cuff: imaging characteristics and comparison of ABER view with oblique coronal view at MR arthrography initial results. *Radiology.* 2002;224(2):470-476.
30. MacGillivray JD, Fealy S, Potter HG, O'Brien SJ. Multiplanar analysis of acromion morphology. *Am J Sports Med.* 1998;26(6):836–840.
31. Madden ME. The magic-angle effect of the supraspinatus tendon. *Radiol Technol.* 2006;77(5):357-365.
32. Maffet MW, Gartsman GM, Moseley B. Superior labrum-biceps tendon complex lesions of the shoulder. *Am J Sports Med.* 1995;23(1):93-98.
33. Mengiardi B, Pfirrmann CWA, Gerber C, Hodler J, Zanetti M. Frozen shoulder: MR arthrographic findings. *Radiology.* 2004;233(2):486-492.
34. Mohana-Borges AVR, Chung CB, Resnick D. Superior labral anteroposterior tear: classification and diagnosis on MRI and MR arthrography. *Am J Roentgenol.* 2003;181(6):1449-1462.
35. Morag Y, Bedi A, Jamadar DA. The rotator interval and long head biceps tendon: anatomy, function, pathology, and magnetic resonance imaging. *Magn Reson Imaging Clin N Am.* 2012;20(2):229-259, x.
36. Neer CS. Replacement arthroplasty for glenohumeral osteoarthritis. *J Bone Joint Surg Am.* 1974;56(1):1-13.
37. Neviaser TJ. The anterior labroligamentous periosteal sleeve avulsion lesion: a cause of anterior instability of the shoulder. *Arthroscopy.* 1993;9(1):17-21.
38. Neviaser TJ. The GLAD lesion: another cause of anterior shoulder pain. *Arthroscopy.* 1993;9(1):22-23.
39. Opsha O, Malik A, Baltazar R, et al. MRI of the rotator cuff and internal derangement. *Eur J Radiol.* 2008;68(1):36-56.
40. Pearle AD, Warren RF, Rodeo SA. Basic science of articular cartilage and osteoarthritis. *Clin Sports Med.* 2005;24(1):1-12.
41. Perthes G. Über Operationen bei habitueller Schulterluxationen. *Deutsches Zeitschrift Chirurgie.* 1906;85:199-227.
42. Pfirrmann CW, Zanetti M, Weishaupt D, Gerber C, Hodler J. Subscapularis tendon tears: detection and grading at MR arthrography. *Radiology.* 1999;213(3):709-714.
43. Pfirrmann CWA, Hodler J. MRT der Schulter. *Radiologie up2date.* 2001;1:125-141.
44. Rudez J, Zanetti M. Normal anatomy, variants and pitfalls on shoulder MRI. *Eur J Radiol.* 2008;68(1):25-35.
45. Sanders TG, Tall MA, Mulloy JP, Leis HT. Fluid collections in the osseous tunnel during the first year after anterior cruciate ligament repair using an autologous hamstring graft: natural history and clinical correlation. *J Comput Assist Tomogr.* 2002;26(4):617-621.
46. Sanders TG, Zlatkin M, Montgomery J. Imaging of glenohumeral instability. *Semin Roentgenol.* 2010;45(3):160-179.
47. Saupe N, White LM, Bleakney R, et al. Acute traumatic posterior shoulder dislocation: MR findings. *Radiology.* 2008;248(1):185-193.
48. Schaeffeler C, Mueller D, Kirchhoff C, Wolf P, Rummeny EJ, Woertler K. Tears at the rotator cuff footprint: prevalence and imaging characteristics in 305 MR arthrograms of the shoulder. *Eur Radiol.* 2011;21(7):1477-1484.
49. Schreinemachers SA, van der Hulst VPM, Willems WJ, Bipat S, van der Woude H-J. Detection of partial-thickness supraspinatus tendon tears: is a single direct MR arthrography series in ABER position as accurate as conventional MR arthrography? *Skeletal Radiol.* 2009;38(10):967-975.
50. Seeger LL, Gold RH, Bassett LW, Ellman H. Shoulder impingement syndrome: MR findings in 53 shoulders. *Am J Roentgenol.* 1988;150(2):343-347.
51. Snyder SJ, Karzel RP, Del Pizzo W, Ferkel RD, Friedman MJ. SLAP lesions of the shoulder. *Arthroscopy.* 1990;6(4):274-279.
52. Sofka CM, Ciavarra GA, Hannafin JA, Cordasco FA, Potter HG. Magnetic resonance imaging of adhesive capsulitis: correlation with clinical staging. *HSS J.* 2008;4(2):164-169.
53. Sofka CM, Lin J, Feinberg J, Potter HG. Teres minor denervation on routine magnetic resonance imaging of the shoulder. *Skeletal Radiol.* 2004;33(9):514-518.
54. Speed CA, Hazleman BL. Calcific tendinitis of the shoulder. *N Engl J Med.* 1999;340(20):1582-1584.

55. Tirman PF, Bost FW, Garvin GJ, et al. Posterosuperior glenoid impingement of the shoulder: findings at MR imaging and MR arthrography with arthroscopic correlation. *Radiology.* 1994;193(2):431-436.
56. Tirman PF, Bost FW, Steinbach LS, et al. MR arthrographic depiction of tears of the rotator cuff: benefit of abduction and external rotation of the arm. *Radiology.* 1994;192(3):851-856.
57. Tuite MJ. Magnetic resonance imaging of rotator cuff disease and external impingement. *Magn Reson Imaging Clin N Am.* 2012;20(2): 187-200, ix.
58. Tuite MJ. MR imaging of sports injuries to the rotator cuff. *Magn Reson Imaging Clin N Am.* 2003;11(2):207-219, v.
59. Walch G, Ascani C, Boulahia A, Nové-Josserand L, Edwards TB. Static posterior subluxation of the humeral head: an unrecognized entity responsible for glenohumeral osteoarthritis in the young adult. *J Shoulder Elbow Surg.* 2002;11(4):309-314.
60. Walch G, Liotard JP, Boileau P, Noël E. Postero-superior glenoid impingement. Another impingement of the shoulder [in French]. *J Radiol.* 1993;74(1):47-50.
61. Walch G, Nové-Josserand L, Boileau P, Levigne C. Subluxations and dislocations of the tendon of the long head of the biceps. *J Shoulder Elbow Surg.* 1998;7(2):100-108.
62. Weishaupt D, Zanetti M, Exner GU. Familial occurrence of glenoid dysplasia: report of two cases in two consecutive generations. *Arch Orthop Trauma Surg.* 2000;120(5-6):349-351.
63. Weishaupt D, Zanetti M, Tanner A, Gerber C, Hodler J. Lesions of the reflection pulley of the long biceps tendon. MR arthrographic findings. *Invest Radiol.* 1999;34(7):463-469.
64. Williams MM, Snyder SJ, Buford D. The Buford complex—the "cord-like" middle glenohumeral ligament and absent anterosuperior labrum complex: a normal anatomic capsulolabral variant. *Arthroscopy.* 1994;10(3):241-247.
65. Zanetti M, Carstensen T, Weishaupt D, Jost B, Hodler J. MR arthrographic variability of the arthroscopically normal glenoid labrum: qualitative and quantitative assessment. *Eur Radiol.* 2001;11(4):559-566.
66. Zanetti M, Gerber C, Hodler J. Quantitative assessment of the muscles of the rotator cuff with magnetic resonance imaging. *Invest Radiol.* 1998;33(3):163-170.
67. Zanetti M, Weishaupt D, Gerber C, Hodler J. Tendinopathy and rupture of the tendon of the long head of the biceps brachii muscle: evaluation with MR arthrography. *Am J Roentgenol.* 1998;170(6):1557-1561.
68. Zubler C, Mengiardi B, Schmid MR, Hodler J, Jost B, Pfirrmann CWA. MR arthrography in calcific tendinitis of the shoulder: diagnostic performance and pitfalls. *Eur Radiol.* 2007;17(6):1603-1610.